NASA Contractor Report 201696

Low Frequency Vibration Characteristics of the Commercial Refrigeration/Incubation Module

James W. Russell and Mehzad Javeed
Lockheed Martin Engineering & Sciences, Hampton, Virginia

Contract NAS1-19000

May 1997

National Aeronautics and
Space Administration
Langley Research Center
Hampton, Virginia 23681-0001

LOW FREQUENCY VIBRATION CHARACTERISTICS OF THE COMMERCIAL REFRIGERATION / INCUBATION MODULE

James W. Russell and Mehzad Javeed
Lockheed Martin Operations Support
Hampton, Virginia

May 1997

ABSTRACT

This report summarizes the results of force and moment measurements of the Commercial Refrigeration /Incubation Module (CRIM) over the frequency range from 0.35 Hz to 300 Hz. In addition to measuring the low frequency vibration characteristics, mass property measurements were performed on both the stand-alone CRIM with the D cell batteries installed as well as the CRIM integrated with the low frequency vibration test platform. This report summarizes the results of the weight, center of gravity, and moments of inertia on three orthogonal axes. The CRIM operates by transferring heat to or from the left wall of the payload chamber to the airflow that passes next to the plate. Thermoelectric control devices (TEDs) are employed to heat or cool this control wall. Measurements were made for the four different CRIM operating regimes and the operating modes of the two banks of TEDs. The CRIM operating regimes include cooling below room temperature, cooling above room temperature, heating below room temperature, and heating above room temperature. There are three TEDs in each bank. At low heat transfer rates the two banks operate in series to reduce the voltage. At high heating rates the two banks of TEDs operate in parallel. The CRIM was mounted to the test apparatus in the same manner as it would be mounted to the middeck or a Space Station EXPRESS rack. The vibration test results showed that the primary forces and moments occurred at frequencies between 68 Hz and 69 Hz, which is the operating speed of the fan that controls the airflow. The results also showed that the operating regime of the CRIM and the operating mode of the banks of TEDs did not significantly affect the maximum forces and moments that were associated with the fan operating speed. The peak force of 0.021 pounds occurred on the Y axis and the maximum moment of 0.14 inch pounds occurred on the Z axis. The results also show an anomaly in the CRIM force and moment measurements. The forces and moments associated with test points taken after the CRIM was turned off and turned back on due to a thermal fuse overload, were significantly higher than the forces and moments associated with test points taken prior to this shutdown. It was recommended that additional testing be performed on the CRIM to investigate this phenomenon.

ACKNOWLEDGEMENTS

This work was performed at NASA Langley Research Center as part of contract NAS1-19000 under the guidance of Mr. George F. Lawrence and Dr. L. Bernard Garrett of the Utilization and Analysis Branch. The authors thank Dr. Howard M. Adelman and Dr. Michael G. Gilbert of the Structural Dynamics Branch for providing facility support and technical expertise in the operation of the Low Frequency Vibration Test apparatus. The authors also recognize Mr. Burnie S. Williams and Mr. David G. Kessler of the Structures and Materials Research Branch for their assistance in the setup of the test apparatus. Lastly, the authors recognize Mr. Craig Savchenko of Wyle Laboratories for his technical expertise in the implementation of the data acquisition system.

TABLE OF CONTENTS

INTRODUCTION

The test results presented herein document the low frequency vibration characteristics of Serial No. 0005 Commercial Refrigerator / Incubation Module (CRIM) part number 12380-501. The CRIM was provided by the Center for Macromolecular Crystallography at the University of Alabama at Birmingham. The CRIM is a fully qualified space hardware item that was developed by Space Industries, Inc. to provide a thermally controlled environment for spaceborne payloads. The CRIM is designed to be mounted in the Space Shuttle middeck and in the Space Station EXPRESS Rack. The CRIMs are used by UAB for growing protein crystals in space. When the CRIM is operating in the refrigeration mode, thermoelectric devices (TEDs) pump heat from the payload. A small high performance fan draws air into a heat exchanger through an air inlet screen on the front of the CRIM. The air removes the heat from the finned heat sink on the hot side of the TEDs. The heated air passes through the fan, and is exhausted through two air exhaust screens at the rear left side of the CRIM. When the CRIM is operating in the heating or incubation cycle mode, heat is extracted from the ambient air and passed through the TEDs and into the payload chamber.

The movement of air through the CRIM combined with the operation of the fan motor are disturbance sources that could affect the microgravity environment in an EXPRESS rack. Furthermore the EXPRESS rack has room for eight middeck locker experiments that are the same size as the CRIM. In fact, the EXPRESS rack could contain several CRIM type experiments that may be operating simultaneously.

Therefore, the purpose of the NASA Langley low frequency vibration tests were to determine the disturbance source characteristics of a CRIM in terms of both forces and moments for evaluation by the EXPRESS rack facility developer.

EQUIPMENT DESCRIPTION

The equipment description includes the test apparatus, the data acquisition system and the Commercial Refrigeration / Incubation Module, and CRIM interface plate.

Test Apparatus

The low frequency vibration test apparatus (LFVTA) configuration components consist of the test platform and the suspension system. Figure 1 shows a photograph of the test apparatus platform. Figures 2a through 2c show the dimensions and layout of the test platform. The test platform consists of a 21 inch diameter 1.973 inch thick aluminum plate mounted under a hollow truncated aluminum cone that has a 9.5 inch diameter base, a 5.5 inch diameter top, is 10 inches tall, and has 1.5 inch thick wall. On top of the cone is a 1 inch diameter, 0.5 inch thick boss that provides a mounting place for the suspension of the platform. The cone is attached to the suspension cable by a u-bolt and an eye bolt that is threaded into the top of the cone. There are 10 QA-700 Allied Signal micro-g accelerometers mounted onto the LFVTA using five mounting blocks that are 1.5 inch aluminum cubes. Table 1 and Figures 2a through 2c summarize the location of the 10 accelerometers. Two accelerometers are mounted inside the top of the cone on a mounting block that is centered on the cone axis. These accelerometers are aligned along the X and Y axes and are 8 inches above the top surface of the 21 inch aluminum plate. The other four mounting blocks are mounted 90 degrees apart to the top of the aluminum plate along the X and Y axes at a radius of 8 inches. On top of each of the four mounting blocks is a Z axis accelerometer. On each of the two Y axes mounting blocks is an accelerometer that is oriented in the X direction. On each of the two X axes mounting blocks are two accelerometers that are oriented in the Y direction. Each accelerometer has four wires that are taped to the plate and cone and are attached to a 50 pin connector that is part of the mass of the LFVTA. The mass of the LFVTA platform with the accelerometers and the wiring is 98.4 pounds.

The suspension system consists of the Zero Spring Rate Mechanism (ZSRM), a turnbuckle, and the suspension cable. The ZSRM allows for suspension of large masses at very low spring rates. The ZSRM compensates for the stretching of the main spring by the contraction of a side spring and visa versa. Figure 3 shows a schematic of the test apparatus including the suspension system. The ZSRM was modified by employing four 1.750 inch diameter 9 inch long stainless steel extension springs that have spring constants of 4.4 pounds per inch and maximum loads of 64 pounds each. Also the top and bottom main spring support bars were each replaced by 1.00 inch high, 11.15 inch long, 0.25 inch wide aluminum plate. The support bars were designed to mount to the ZSRM. The side springs were the 0.5 inch diameter springs supplied with the ZSRM. The natural frequency of the test platform in the Z direction was less than 0.25 Hz.

The suspension cable is a 0.065 inch diameter 39 foot 9 inch long Vectran HS T-97 cable that has a load carrying capacity of 500 pounds. The cable is attached to the ZSRM with a turnbuckle to allow height adjustments of the test platform. The test platform is suspended from the bottom of the Vectran cable with a u-bolt. The bottom of the 21 inch diameter test plate is 15.4 inches below the end of the suspension cable.

Data Acquisition System

Figure 4 shows a schematic of the data acquisition system. The signal processing equipment includes two 6 channel Servo Accel Signal Conditioners, a Precision Filters Model 416 Filter/Amplifier and a Gateway 2000 PS-166 Mhz Pentium computer. The 10 micro-g accelerometers were powered by a ±15 volt DC power supply in the Servo Accel 85 signal conditioners that were fabricated by the Instrument Research Division of NASA Langley Research Research Center. The accelerometers were calibrated with the signal passing through the Servo Accel 85 signal conditioners. For accelerometer calibration the signal was not amplified except for the external resistors that are located in the Servo Accel 85 signal conditioners. The acceleration levels were nominally set at 5 volts per g.

The Servo Accel 85 signal conditioners provided a reference voltage to minimize the DC acceleration signal.

The output signals from the Servo Accel 85 signal conditioners were fed into the Precision Filters Model 416 Filter/Amplifiers. In addition to the gain on the Servo Accel the Model 416 Filter/Amplifiers contain a prefilter amplifier, a low pass filter, and a post filter amplifier for each channel. The frequency range measured was from 0 to 300 Hz and the frequency resolution was 0.29297 Hz. The prefilter amplifier for all channels was set to 1 and the post filter amplifier was set to 10.

Commercial Refrigeration / Incubation Module

Figure 5 shows a picture of the CRIM. The outside dimensions of the CRIM unit are 19.83 inches long, 18.08 inches wide, and 10.60 inches high. It has a back and front cover plate that are 10.60 inches high and 18.08 inches wide with large rounded corners. Between the cover plates are a top and bottom plate that are cut in 2.21 inches from both the right and left sides. The side plates are cut in 2.21 inches from both the top and bottom plates. At each of the four corners a 3.12 inch wide plate is placed along the length between the end plates at a 45 degree angle such that it connects the top or bottom plate with the side plate. The purpose of this octagonal shape is to provide room for an extended nut driver to bolt the CRIM to the middeck or the Express rack. The nominal weight of the CRIM without batteries is 36.5 pounds. Reference 1 provides a more detailed description of the CRIM as well as the operating characteristics.

The CRIM electronics includes a battery pack that contains two 1.5 volt D cell batteries. The battery pack allows the electronics to continue logging data in the CRIM data logger any time there is a CRIM power failure. Under battery power, the active thermal control system will not operate and the software cannot be accessed by the user.

Thermal Control System. - Thermal insulation is used between the outer aluminum sheet walls and the inner aluminum sheet walls. The front cover plate of the CRIM employs a swing door front panel that allows payloads to be placed in the CRIM. The front door also has the switches for operating the CRIM and the LCD for monitoring the CRIM operation or displaying the CRIM input control values.

The temperature of the payload left side inner wall is controlled by two banks of thermoelectric devices (TEDs). Each bank has three TEDs. If the required heat flow rate is low, then the two banks of TEDs are operated in series such that the voltage drop across each TED is small. This low voltage operation provides for very precise temperature control. If the required heat flow is high, then the two banks of TEDs are operated in parallel, such that the voltage drop across each TED is high and the heat pumping capacity is significantly increased.

There are nine plate type thermistors that the user can place in the payload and can be used in any combination as the control thermistors. Temperature values from the control thermistors are used by the CRIM software for controlling the thermal control system. A tenth thermistor is used for measuring the inlet air temperature.

Power Requirements. - The CRIM requires a constant 28 DC volt power supply that can provide current from 0.4 to 4.6 amperes. The high amperage occurs when the thermal control system is active. The CRIM will provide up to 0.85 Amperes at 28 Vdc to the payload. The fan voltage ranges from 22 Vdc to 28 Vdc and the fan current varies from 0.2 A to 0.4 A. The electronics are powered through a 5 Vdc DC/DC converter and can draw up to 0.2 A.

Software System. - The software for operating the CRIM is controlled by four push buttons located on the front panel of the CRIM. The CRIM uses a 4 row 40 column LCD in the top center of the front panel to display CRIM information and command options that are numbered to correspond to the push button. The CRIM software employs fuzzy logic for operating the thermal control system. The software limits the temperatures and thermal cycling of the TEDs.

CRIM Interface Plate. - Figure 6 shows the dimensions of the CRIM interface plate. The interface plate is a 0.5 inch thick aluminum plate that is 20 inches long and 13 inches wide. It has four lightning holes that are 6 inches long and 4 inches wide and have a 0.50 inch radius at each corner. The mass of the interface plate alone is 7.94 pounds and the attachment weight is 0.524 pounds. The CRIM is mounted to the test apparatus using an interface plate that was drilled to match both the hole locations of the test apparatus and the CRIM. The holes in the interface plate for the CRIM attachment bolts are located such the X axis of the CRIM is aligned with the Z axis of the test platform and the Y axis of the CRIM is aligned with the Y axis of the test apparatus. Thus the Z axis of the CRIM is aligned with the X axis of the test apparatus. In addition the center of gravity (CG) of the of the CRIM and the interface plate are very close to the center of gravity of the test apparatus in the XY plane. Figure 7 shows the installation of the CRIM on the test apparatus.

The interface plate was designed such that it is adaptable to other middeck and EXPRESS rack payloads. These other payloads can be accommodated by simply drilling additional payload mounting holes in the interface plate, such that the CG of the payload is aligned with the CG of the test apparatus.

CENTER OF GRAVITY AND MOMENTS OF INERTIA

Moment of inertia (MOI) and CG measurements were previously made on all three axes of the test apparatus using the Space Electronics Mass Properties Instrument Model KSR1320-1500. MOI and CG measurements were made for the stand alone CRIM and the CRIM integrated with the test apparatus and the interface plate attached. Table II summarizes the measurements. The moments of inertia of the CRIM are 1,610.2 $lb\text{-}in^2$ on the X axis, 2,007.2 $lb\text{-}in^2$ on the Y axis, and 2,799.8 $lb\text{-}in^2$ on the Z axis.

The CRIM was mounted to the test apparatus such that the X axis of the CRIM is aligned with the Z axis of the test apparatus. The CRIM was mounted such that the Y axis of the CRIM is aligned with the Y axis of the test apparatus, and the Z axis of the CRIM is aligned with the X axis of the test apparatus. Table II shows that the MOI measurements of the CRIM integrated to the test platform are 10,857 $lb\text{-}in^2$ on the X axis, 9,892 $lb\text{-}in^2$ on the Y axis, and 6,201 $lb\text{-}in^2$ on the Z axis.

Table II shows that for the test apparatus, the X axis and Y axis CG locations are within 0.04 inches of the center of the plate. The Z axis CG location for the test apparatus alone is 2.774 inches above the bottom surface of the plate. The X axis CG location of the installed CRIM is within 0.592 inches of the center of the plate and the Y axis CG location is within 0.10 inches of the center of the plate. The Z axis CG location of the installed CRIM is 10.14 inches below the bottom surface of the test apparatus platform circular plate. Thus for the test apparatus with the CRIM installed the X axis and Y axis CG locations are within 0.15 inches and 0.02 inches of the center of the circular plate. The Z axis CG is 0.8 inches below the bottom center of the plate.

To provide a check of the validity of the measurements, the MOI and CG of each component that makes up the integrated CRIM test assembly was measured or computed. Table III shows a summary of the moments of inertia of the test apparatus platform, the CRIM, the interface plate, and the assembly. The moments of inertia of the interface plate were calculated using the mass properties program (reference 2). Also shown in Table III are the moment of inertia offset corrections from the CG of each component to the CG of the system. The CRIM interface plate and attachment bolts were weighed and the CGs were calculated to be in the middle of the plate for the X and Y axes. The Z axis CG for the interface plate was calculated using the mass properties program. The Z axis CG for the bolts were assumed to be at the middle of the bolt. The CGs of the CRIM, the interface plate, and the bolts were corrected from the component reference axis system to the test apparatus platform reference axis system.

For the test apparatus alone, the moment of inertia about the Y axis is 0.4 percent (17 $lb\text{-}in^2$) greater than the moment of inertia about the X axis. These small discrepancy results from imperfections in the machining and assembly of the test apparatus platform, offset of the two accelerometers located inside the cone, and the offset of the 50 pin accelerometer signal connector. The moment of inertia of the Z axis is almost 75 percent higher than either the X or Y moment of inertia for the test apparatus. With the CRIM and CRIM interface plate installed the moments of inertia of the system increase more than 100 percent for both the X and Y axes. The Z axis increase is a little more than 50 percent. The effect of the CRIM on the location of the Z axis CG significantly increases the moments of inertia about the X and Y axes.

OPERATION OF COMMERCIAL REFRIGERATION / INCUBATION UNIT

A power supply was provided by UAB that generated up to 28 DC volts and 5 amperes was used to operate the CRIM unit. A 10 foot extension cable was fabricated to increase the cable length between the power source and the CRIM. This extension provided a means to suspend the cable from above, so that the cable can freely move short distances in all three directions. With this flexible cable system, the forces transmitted from the CRIM through the cable are minimized. The mass properties used in the analysis do not include the slight increase in mass associated with the cable connector mounted to the front of the CRIM.

Operation of the CRIM involves turning the power on, and setting the desired temperature of the response thermistor and monitoring the heat transfer rates into the control plate. The CRIM outputs the heat transfer rates in terms of QB counts. The only heat conduction path from the control plate to the response thermistor is through the circulating air system in the payload area. The rate of heat flow to the control plate is controlled by the control plate thermistor temperature and the response thermistor temperature through a fuzzy logic system.

For this test, the response thermistor temperature did not vary significantly from room temperature. Thus the control plate temperature varied considerably in a relatively short time in order to get the response thermistor temperature to the desired level. As the control plate temperature increases or decreases, the difference between the control plate temperature and the response thermistor temperature increases. Therefore, as the control plate temperature increases, the heat transfer rates are required to increase in order to adjust the response thermistor temperature to the desired level. Thus, the QB counts increase as the control plate temperature varies from room temperature. Figure 7 shows the variation of QB counts with the control plate temperature. The maximum QB count level is 256 and the temperature limits are 4° C on the cold side and 40° C on the hot side. Room temperature is approximately 22° C. Because of the fuzzy logic, the temperature is more or less a band rather than the single line shown on Figure 7. At low QB levels the two banks of TEDs operate in parallel with a low voltage drop. As the QB counts increase to 151, the controller relays switch the operating mode of the two banks of TEDs from series to parallel. This larger voltage drop across each TED allows significantly higher heat transfer rates. Similarly, as the QB counts decrease the controller relay switches the operating mode of two banks of TEDs from parallel to series.

TEST PROCEDURE AND DATA PROCESSING

The CRIM test series included taking background vibration measurements before and after taking vibration measurements of the CRIM at various operating conditions. Low frequency vibration measurements of the CRIM were made at various heat transfer points where the two banks of TEDs were in series, in parallel, transition from series to parallel, and transition from parallel to series. After taking the background measurements, the CRIM power was turned on and an initial data point was taken. Then the CRIM response thermistor temperature was set to 4° C and data points were taken when the QB count reached 80 with the TED banks in series, when the QB count reached 145 where the TED banks switch from series to parallel, and when the QB count reached 210 with the TED banks in parallel.

Following this last measurement where the control plate temperature was near 8° C, the response thermistor was manually set to 40° C, and the CRIM continued to operate. Data points were taken when the QB count decreased and again reached 210 with the TEDs in parallel, when the QB count decreased to 160 where the TED banks switch from parallel to series, when the QB count reached 80 with the TED banks in series. The control plate temperature was still below room temperature for these test points. As the fuzzy logic controller continued to adjust the heat flow into the control plate, the control plate temperature adjusted. When the cold plate temperature was near room temperature there was virtually no heat flow. When the QB count decreased to 10, another data point was taken. The control plate temperature now started to go above room temperature in order to get the response thermistor temperature to 40° C. Data points were taken when the QB count reached 80 with the TED banks in series, when the QB count reached 145 where the TED banks switch from series to parallel, and at 210, with the TED banks in parallel. At the end of this data point, the control plate temperature was over 35° C.

Again the response temperature was manually set to 4° C and the CRIM continued to operate. The first data point taken when the QB count reached 160 counts. This was the point where the TED banks transition from parallel to series. The next data points were taken when the QB count reached 80 with the TED banks in series and the last data point was taken when the QB count reached 10. Table IV lists the test point numbers, the response thermistor temperature setting, the QB count range, the associated control wall temperature, and the operation mode of the two TED banks.

Table IV lists additional test points. The CRIM was cycled through the various operating ranges a second time. For the second series the initial temperature setting for the response thermistor was 40° C, so that the control plate temperature was driven to the hot side first. After getting the data point at the QB count of 210, the response thermistor temperature was set to 4° C, and the CRIM was allowed to run. However, the CRIM LCD indicated a thermal fuse was open, and the unit was shut down to cool. This cooling involved opening the front panel to cool the control plate and letting the unit sit for approximately 30 minutes. The front panel was then closed, the power was turned on, and the response thermistor temperature was set to 4° C. The CRIM unit was then cycled through room temperature down to the cold side and back to near room temperature. After this last data taken near room temperature, the power was turned off and a last data point was taken. Sometime later, a background vibration measurement was made.

Table IV shows that the QB levels vary during the test point measurement. This is because each test point consists of 61.5 seconds of data. The data is sampled at 1200 Hz for each of the 10 accelerometers. The data acquisition system consists of a multifunction input/output board that acquires the amplified accelerometer output signals. The PS166 computer is then programmed in LABVIEW to process and record the accelerometer data in text format. The text format files are then transferred to a work station machine for analysis. The text files are copied into a universal file format and windowed using a FORTRAN program. The window program removes the DC offset from each accelerometer channel and uses a 4 sample Kaiser Bessel window to process small sections of the total data set of each accelerometer. The window program employed a 50 percent overlap for each small data set. The universal windowed data was then entered into I-DEAS to convert the data from the time domain to the frequency domain. This conversion involves converting each of the windowed data sets and then averaging the amplitudes and phase angles at each discrete frequency for each accelerometer over the range from 0 to 300 Hz. FORTRAN programs were then used to correct the frequency domain data for the accelerometer calibrations, remove the background vibration levels, compute the forces and moments for each of the three axes, remove the test apparatus anomalies including suspension system effects, and compute one-third octave band forces and moments. Figure 8 shows the steps used in processing the data.

RESULTS

The data analysis results consisted of computing power spectral densities (PSDs) and one third octave bands (OTOBs) for the background and for each of the test data points on each of the three axes for both forces and moments. There are 31 sets of PSD and OTOB data covering the frequency range from 0.35 to 300 Hz. The force PSDs are in pounds squared per Hz (lb^2/Hz) and the moment PSDs are in pounds squared times inches to the fourth power per Hz ($[lb\ in^2]^2/Hz$). The OTOB force is in pounds (lb) and the OTOB moments are in pounds times inches squared ($lb\ in^2$). The results include force and moment PSDs and OTOBs for the background test points and two sample test points. In addition forces and moments are presented for the peak OTOB center band frequency of 63 Hz for all test points. The frequencies where the peak forces and moments occur are presented for all test points.

Background Measurements

The background measurements includes test point 31 that was taken prior to testing the CRIM and test point 65 that was taken after the CRIM tests were completed. Figures 10 and 11 show the PSDs for forces and moments respectively on all three axes for test point 31. The bandwidth for the PSDs is 0.29297 Hz, Figure 10 shows that maximum force PSDs on the X and Y axes are at 120 Hz, 180 Hz, and 240 Hz. These are associated with the 60 Hz facility power signal. On the Z axis the maximum background force PSDs occur at 22 Hz, 60 Hz, 129 Hz, and 180 Hz. In addition to the facility power signal, the natural frequency of the suspension cable in the Z direction is 22 Hz. Figure 11 shows that the maximum PSD moments about the X and Y axis are associated with the 22 Hz suspension cable vibration, and the 120 Hz, 180 Hz, and 240 Hz facility power signals. Figure 11 shows that the background moment about Z axis is very low.

Figures 12 and 13 show the OTOB forces and moments respectively on all three axes for test point 31. Figure 12 shows that on the X axis there is a peak force associated with the 1.6 Hz and 2.0 Hz frequencies. This force is caused by the rocking motion of the large mass of the test platform and CRIM on the end of the 40 foot suspension cable. The mass is suspended from the end of the cable with a U-bolt and is allowed to rock freely. Also on the X, Y, and Z axes, there are peak forces associated with the 120 Hz signals. On the Z axis there is also the one third octave band force associated with the 22 Hz suspension cable frequency. Figure 13 shows that the peak moment occurs on the Y axis at the 1.6 Hz and 2.0 Hz, which again is associated with the rocking motion of the large mass at the end of the suspension cable. Also Figure 13 shows peak moments on the X and Y axes at 120 Hz. The peak moment on the Z axes occurs at 60 Hz.

Figures 14 through 17 show the force PSDs, the moment PSDs, the OTOB forces, and the OTOB moments for background test point 65. The force PSDs for test point 65 shown on Figure 14 are similar to those shown on Figure 10 for test point 31. On the X axis, test point 65 has more noise in the range between 75 Hz and 130 Hz and does not show a significant signal at 240 Hz. On the Y axis, test point 65 shows a disturbance at 22 Hz. The Z axis disturbances are similar for both background test points.

A comparison of the moment PSDs for test point 65, Figure 15, with the moment PSDs for test point 31, Figure 11, shows that on the X and Y axes, the 22 Hz moment is greater for test point 65. Also there are high vibration levels in the range from 93 Hz to 130 Hz on the Y axis for test point 65. The Z axis on Figure 15 shows a 120 Hz signal for test point 65 that is not seen on Figure 11.

A comparison of the OTOB forces for test point 65 shown on Figure 16 with the OTOB forces for test point 31 on Figure 12, show that the two are very similar. The non-peak OTOB forces are higher on all three axes for test point 65. Similarly, a comparison of the OTOB moments for test point 65 shown on Figure 17, with the OTOB moments for test point 31 shown on Figure 13, shows that the moments are very much the same on all three axes.

Sample Test Results

Figures 18 through 25 present the force PSDs, the moment PSDs, the force OTOBs, and the moment OTOBs for test points 38 and 51. The selection of these test points was arbitrary. Test point 38 is a test point where the control wall temperature is being reduced from near 40° C to 4°C and the two banks of TEDs are in parallel. Figure 18 shows the force PSDs for the X, Y, and Z axes for test point 38. The figure shows that there is a dominant force near 68 Hz on the X and Y axis. It is not quite as dominant on the Z axis. Also there are vibrations at frequencies above 250 Hz on the Y axis. Figure 18 also show that there is a force at a frequency near 1.4 Hz on both the X and Y axes. Associated with these forces are the moments. Figure 19 shows the moment PSDs for test point 38 on the X, Y, and Z axes. The dominant moment appears to be at 68 Hz on all three axes. The moment on the Z axes at 68 Hz is greater than the X and Y moments. This is because the forces are larger on the X and Y axes and result in a larger moment about the Z axis. Again there are moments on the X and Y axes near 1.4 Hz. Also the X axes moments are large above 250 Hz.

As mentioned previously, the forces and moments at 1.4 Hz on the X and Y axes are associated with the rocking of the test apparatus platform and CRIM assembly about the hang point at the bottom of the 40 foot long suspension cable, rather than a direct result of the CRIM operation. The forces and moments at frequencies above 250 Hz may be due to the vibration of the thin aluminum cover plate on the CRIM near the fan. The most significant forces and moments near 68 Hz are associated with the fan speed of the CRIM.

Figure 20 shows the OTOB forces for all three axes for test point 38. This figure shows the dominance of the OTOB center band frequency of 63 Hz on the X and Y axes. The 68 Hz signal is contained in this OTOB. The force is near 0.02 pounds on the X and Y axes. The Z axis force is almost an order of magnitude less. Figure 21 shows the OTOB moments for test point 38. On the X axis, the low frequency moments dominate. Again, it is believed that these are associated with the test apparatus rather than the CRIM. At the 63 Hz OTOB, the moment on the Z axis exceeds the 63 Hz OTOB moments on both the X and the Y axes.

Figure 22 shows the force PSDs for the X, Y, and Z axes for test point 51. Test point 51 is a transition point where the temperature is above room temperature and the control wall is trying to heat the control thermistor to 40° C. The two banks of TEDs are changing from series mode to parallel mode as the QB increases from 145 to 158. Like test point 38, Figure 22 shows that the dominant force for test point 51 is near 68 Hz on the X and Y axis. It is not quite as dominant on the Z axis. Also there are vibrations at frequencies above 250 Hz on both the Y and Z axes. Again it is believed that these high frequency vibrations are associated with the thin aluminum cover on the CRIM.

Associated with these forces are the moments. Figure 23 shows the moment PSDs for test point 51 on the X, Y, and Z axes. Again, the dominant moment appears to be at 68 Hz on all three axes. The moment on the Z axes at 68 Hz is greater than the X and Y moments. This is because the forces are larger on the X and Y axes and result in a larger moment about the Z axis. Also, Figure 23 shows a moment on the Y axis near 1.4 Hz. Like test point 38, the X axes moment PSDs for test point 51 are large above 250 Hz.

Figure 24 shows the OTOB forces for all three axes for test point 51. This figure shows the dominance of the OTOB center band frequency of 63 Hz on the X and Y axes. The force is near 0.02 pounds on the X and Y axes. The Z axis force is almost an order of magnitude less. The low frequency moments near 1.4 Hz on the X axis are not as dominant for test point 51 as they were for test point 38 (Figure 20). Figure 25 shows the OTOB moments for test point 51. Like test point 38, Figure 25 shows that for the 63 Hz OTOB center band frequency, the moment on the Z axis exceeds the 63 Hz OTOB moments on both the X and the Y axes.

The data shown on Figures 18 through 25 for test points 38 and 51 is similar to the data for all the other test points. The data shows that the maximum forces and moments occur at the OTOB center band frequency of 63 Hz.

Peak Forces and Moments at OTOB Center Band Frequency of 63 Hz

The CRIM operating modes were divided into four categories as follows: (1) cooling with the control wall temperature below room temperature, (2) cooling with the control wall temperature above room temperature, (3) heating with the control wall temperature below room temperature, and (4) heating with the control wall temperature above room temperature. Figures 26, 27, and 28 show the peak forces at each of the conditions on the X, Y, and Z axes respectively. Figure 26 shows that for the X axis the OTOB force associated with the 63 Hz center band frequency is 0.005 pounds for all test points prior to test point 52. At all test points of 52 and above, the peak force increases to 0.10 pounds. The numbers above the data represent the average QB value for the test point. As mentioned previously, if the QB is less than 145 the two banks of TEDs are in series; if the QB values are above 160, the two banks of TEDs are in parallel; and if the QB value is near 150, the two banks of TEDs are transitioning from series to parallel or from parallel to series. Figure 26 shows that there is very little variation between the various test points and that the peak X force is not affected by operating condition or the mode of operation of the TEDs.

A review of Table IV that presents the test points, shows that after test point 52 there was a thermal fuse overload. The CRIM was turned off, the front door was opened, and the unit was cooled down at room temperature for approximately 30 minutes. The door was closed, and the unit was turned on. For all test points that occurred after this shutdown and test point 52, the forces increased by approximately 100 percent as shown on Figure 26. The reason for this increase is not understood.

Figure 27 shows the peak forces on the Y axis at the OTOB center band frequency of 63 Hz for each test point. Again the test points are divided into the four CRIM operating modes. The peak forces on the Y axes vary between 0.07 and 0.08 pounds prior to test point 52. For test points taken after test point 51 the peak Y forces doubled to 0.014 to 0.015 pounds. These peak Y forces are approximately 50 percent higher than the peak forces on the X axis. Like the X axis, the operating mode of the TEDs did not affect the peak forces.

Figure 28 shows the peak forces on the Z axis for each test point at the OTOB center band frequency of 63 Hz. The peak forces on the Z axis are less than 0.04 pounds, which is considerably less than the peak forces on the X and Y axes. This is because the peak force is associated with the CRIM fan speed, and the fan rotates in the X-Y plane. Again the CRIM operating mode and the operating mode of the TEDs had little effect on the peak force in the Z direction. Also, the Z axis forces doubled for all test points after test point 51.

Test points 36, 39, 43, 45, 51, 57, 59, and 63 are the test points where the mode of operation of the TED banks changed from serial to parallel or from parallel to serial. This transition is very short and there is an obvious impulse click that occurs when the transition takes place. The analysis presented here involves averaging data in three second increments over a period of 54 seconds. Therefore to look at the transition effect, it is recommended that the time history data be plotted, and observe and evaluate the magnitude of any data spike. This would provide a better representation of the transition then the time averaged data.

Figures 29, 30, and 31 show the peak moments at each of the CRIM operating conditions on the X, Y, and Z axes respectively. Figure 29 shows that for the X axis the OTOB moment associated with the 63 Hz center band frequency is 0.02 inch pounds for all test points prior to test point 52. At all test points of 52 and above, the peak moment increases to 0.035 inch pounds. Again, the numbers above the data represent the average QB value for the test point. The figure shows that there is very little variation between the various test points and that the peak X force is not affected by operating condition or the mode of operation of the TEDs.

Figure 30 shows the peak moments at the OTOB center band frequency of 63 Hz for the Y axis. The peak moment for all test points below 52 is 0.015 inch pounds. For all test points above 51, the peak Y axis moment increases to 0.025 pounds. The Y axis moments are less than the X axis moments.

Figure 31 shows the peak moments for the OTOB frequency of 63 Hz for the Z axis. The Z axis moments are 0.05 inch pounds for test points below 52 and 0.10 inch pounds for test points above 51. It is recommended that additional testing be performed to ascertain the reason for the increase in the forces and moments for test points above 51.

The Z axis moments are associated with the forces on the X and Y axes. These forces cause a large moment on the Z axis. Similarly, the small force on the Z axis results in lower moments on the X and Y axes. Figures 26 through 31 show that the CRIM operating forces and moments do not vary with the operating condition of the CRIM or the operating mode of the TED banks.

The narrow band frequency data was reviewed and the particular frequency where the peak X and Y axes forces and the peak Z axes moments occurred for each test point was established. For every test point, the frequency at which the peak Y axis force occurred, was also the frequency where the peak X axis force occurred and the peak Z axis moment occurred. Figure 32 shows the peak forces for each test point on the X, Y, and Z axes. The figure shows that the peak forces occur on the Y axis and at test point 58 the peak force is 0.021 pounds. Figure 33 shows the peak moments for the X, Y, and Z axes for each test point. The moments about the Z axes are considerably greater than the moments about the X and Y axes. Again the peak moment occurs for test point 58 and is 0.14 inch pounds. These peak forces and moments are associated with the operating speed of the CRIM fan.

The operating fan speed was thought to have some variation due to test operating condition and the amount of heat transfer required. Figure 34 shows the operating speed of the fan where the peak forces and moments occurred for each test point. The figure shows that the variation in peak operating speed varies from 68 Hz to 69 Hz. The two frequency humps occur when the response thermistor temperature is transitioned from 4° C to 40° C, which are between test points 37 and 38 and test points 58 and 59.

In addition to showing the peak frequency, the variation of peak force and peak moment with frequency are also presented on Figure 34. The figure shows that the peak forces and moments take place over a frequency range of 1.5 Hz. The frequency band width for this data is 0.29297 Hz.

CONCLUSIONS AND RECOMMENDATIONS

The CRIM mass properties were measured, and the force and moment response levels associated with the CRIM operations were characterized over the frequency range from 0.35 to 300 Hz. Response levels were measured for two complete cooling and heating cycles. The levels associated with the second cycle after the shut down due to the thermal overload switch were consistently higher than the first cycle and the beginning of the second cycle.

The mass property measurements did not include a payload, but did include the two D cell batteries. The weight of the CRIM part no 12380-501 serial no 0005 was 38.06 pounds. The center of gravity using the CRIM reference axis of reference 1 is 9.648 inches on the X axis, 8.432 inches on the Y axis, and 5.610 inches on the Z axis. The moments of inertia about the CG are 1610.2 lb-in^2 about the X axis, 2007.2 lb-in^2 about the Y axis, and 2800.0 lb-in^2 about the Z axis.

The maximum measured forces and moments occurred at frequencies between 68 and 69 Hz. Test point 58 experienced the highest forces and moments. The peak force of 0.021 pounds occurred on the Y axis. The peak moment of 0.14 in-lbs occurred on the Z axis.

The operating condition of the CRIM and the mode of operation of the TEDs did not significantly affect the CRIM forces and moments. The peak frequencies of 69 Hz occurred when the response thermistor temperature transitioned from 4° C to 40° C, which were between test points 37 and 38 and test points 58 and 59.

It is recommended that time history data be analyzed to evaluate the forces and moments associated with the transition of the operating mode of the TED banks from serial to parallel or from parallel to series. Currently the transition regime was obtained by averaging the data over a 61.5 second time span, which tends to wash out the instantaneous transition point.

It is also recommended that this CRIM unit be retested to ascertain the reason for the significant increases in forces and moments after the unit was shut down and restarted because of the thermal overload condition.

REFERENCES

1. "CRIM Commercial Refrigeration / Incubation Module User's Handbook, Version 3.05," Space Industries, division of GB Tech, 101 Courageous Drive, League City, Texas, 77573, July 15, 1996.

2. "Hull, Reid A., Gilbert, John A., and Klich, Phillip J.; "Computer Program for Determining Mass Properties of a Rigid Structure," NASA TM 78681, NASA Langley Research Center, Hampton, VA, March 1978.

TABLE I - Accelerometer Locations and Data Acquisition Channels

ACCELEROMETER IDENTIFICATION					Servo Accel 85 Signal conditioner channel	Precision Filters Model 416 Amplifier channel	Gateway 2000 166 Mhz Pentium channel
Serial number	Measurement axis	Location Coordinates, in X axis	Y axis	Z axis			
12473	X-	0.75	8.00	2.69	1	1	1
12461	Z-	0.00	8.00	3.44	2	2	2
12468	X+	-0.75	-8.00	2.69	3	3	3
12471	Z-	0.00	-8.00	3.44	4	4	4
21561	Y-	8.00	-0.75	2.69	5	5	5
21563	Z-	8.00	0.00	3.44	6	6	6
21565	Y-	-8.00	0.75	2.69	7	7	7
21567	Z-	-8.00	0.00	3.44	8	8	8
12465	X-	0.75	0.00	9.95	9	9	9
12475	Y-	0.00	0.75	9.95	10	10	10

NOTE: Accelerometers are allied Signal QA-700 Micro-g type
Accelerometer locations referenced to bottom center of 21 inch diameter plate

Table II. - Center of Gravity and Moments of Inertia of stand alone CRIM and Crim Integrated with Test Apparatus

CRIM part no. 12380-501 serial no. 0005

MOI Measure	Weight lbs	Center of Gravity X axis in	Center of Gravity Y axis in	Center of Gravity Z axis in	Moment of Inertia X axis lb-in sq	Moment of Inertia Y axis lb-in sq	Moment of Inertia Z axis lb-in sq
Z axis	38.06	9.642	8.412				2799.83
Y axis		9.654		5.581		2007.15	
X axis			8.451	5.639	1610.17		
Average	38.06	9.648	8.432	5.610	1610.17	2007.15	2799.83

C.G. values referenced to CRIM reference point
MOI values referenced to C.G. location

Note: X axis of CRIM is aligned with Z axis of test apparatus
Y axis of CRIM is aligned with Y axis of test apparatus
Z axis of CRIM is aligned with X axis of test apparatus

CRIM MOUNTED TO TEST APPARATUS

MOI Measure	Weight lbs	Center of Gravity X axis in	Center of Gravity Y axis in	Center of Gravity Z axis in	Moment of Inertia X axis lb-in sq	Moment of Inertia Y axis lb-in sq	Moment of Inertia Z axis lb-in sq
Z axis	144.74	-0.1878	-0.0010				6200.70
Y axis			0.0414	-0.807	10856.95		
X axis	144.76	-0.1064		-0.793		9892.12	
Average	144.75	-0.147	0.020	-0.800	10856.95	9892.12	6200.70

C.G. values referenced to bottom center of test apparatus platform
MOI values referenced to C.G. location

Measurements made at NASA Langley Research Center on January 7, 1997 using Mass Properties Instrument Model KSR-1320-1500

TABLE III - Center of Gravity and Moments of Inertia About System Center of Gravity with CRIM Installed

CRIM part number 12380-501 serial number 0005

Component	Weight lb	Center of Gravity in.	MOI about C.G. of part lb-in sq.	C.G. part offset in.	MOI offset correction lb-in sq.	MOI about C.G. of assy lb-in sq
X axis						
test apparatus	98.24	0.0356	3,013.80	-0.1671	1251.08	4,264.88
interface plate	7.936	0	330.15	-0.1315	2.38	332.53
interface bolts	0.524	0	16.76	-0.1315	2.19	18.95
CRIM unit	38.06	-0.592	2,799.83	-0.4605	3,329.76	6,129.59
sum =	144.76	-0.1315				10,745.94
Measurement	144.75	-0.1470				10,856.95
Y axis						
test apparatus	98.24	-0.0201	3,028.00	-0.0326	1253.72	4,281.72
interface plate	7.936	0	135.27	-0.0125	2.51	137.78
interface bolts	0.524	0	16.76	-0.0125	2.20	18.96
CRIM unit	38.06	0.0995	2,007.15	-0.0870	3337.54	5,344.69
sum =	144.76	0.0125				9,783.15
Measurement	144.75	0.0200				9,892.12
Z axis						
test apparatus	98.24	2.7735	4,074.60	3.5685	2.85	4,077.45
interface plate	7.936	-0.248	468.30	0.5470	0.14	468.44
interface bolts	0.524	1.25	0	2.0450	0.01	0.01
CRIM unit	38.06	-10.1480	1,610.17	9.3530	8.36	1,618.53
sum =	144.76	-0.7950				6,164.42
Measurement	144.75	-0.8000				6,200.70

CG position is referenced to bottom center of 21 inch diameter test apparatus plate.
Interface plate values are calculated using massprop program.

Table IV - CRIM Test Point Summary

TEST POINT NUMBER	RESPONSE THERMISTOR SETTING - deg C	HEAT FLOW QB RANGE counts	CONTROL WALL TEMPERATURE deg C	THERMOELECRIC CONTOL DEVICE OPERATION MODE
31	background - off	-	22.0	-
35	4	80 to 91	15.0	series
36	4	145 to 155	12.0	series to parallel
37	4	210 to 218	8.5	parallel
38	40	210 to 192	9.0	parallel
39	40	160 to 142	12.0	parallel to series
40	40	80 to 60	16.0	series
41	40	10 to 0 to 18	20 - 24	series
42	40	80 to 96	29.0	series
43	40	145 to 160	32.0	series to parallel
44	40	210 to 218	35.5	parallel
45	4	160 to 138	32.0	parallel to series
46	4	80 to 57	28.0	series
47	4	10 to 0 to 21	24 - 19	series
48	power off	-	-	-
49	40	10 to 4	20 to 23	series
50	40	80 to 92	29.0	series
51	40	145 to 158	31.0	series to parallel
52	40	210 to 216	35.5	parallel
	thermal fuse overload encountered - unit shut dowr			
53	4	80 to 61	28.0	series
54	4	10 to 0 to 14	24 to 19	series
55	4	80 to 96	15.0	series
57	4	145 to 157	12.0	series to parallel
58	4	210 to 217	8.5	series
59	40	160 to 138	12.0	parallel to series
60	40	80 to 65	15.5	series
61	40	10 to 0 to 13	20 to 24	series
62	40	80 to 105	29.0	series
63	40	145 to 168	32.5	series to parallel
64	power off	-	-	-
65	background - off	-	22.0	-

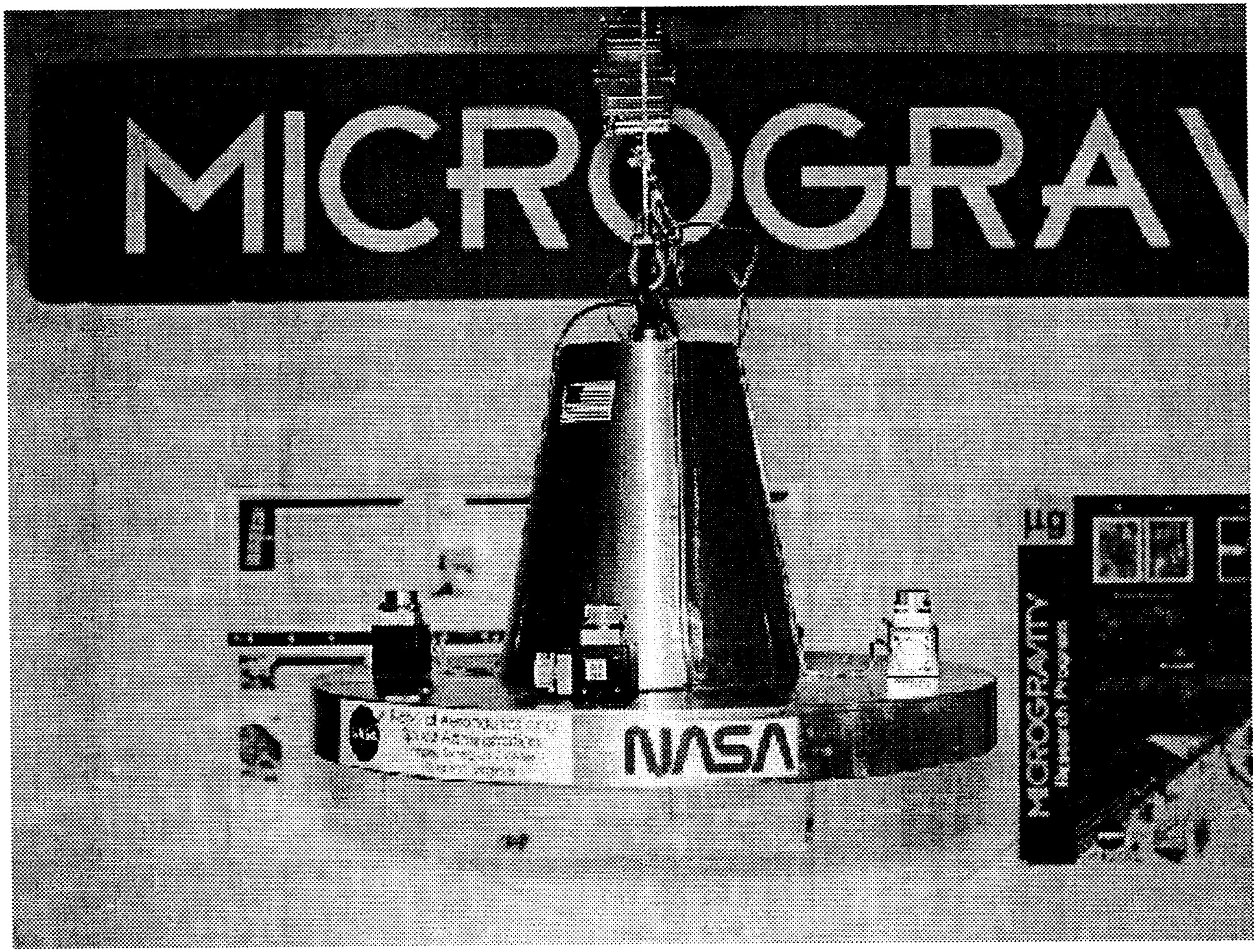

Figure 1. - Test Apparatus Platform

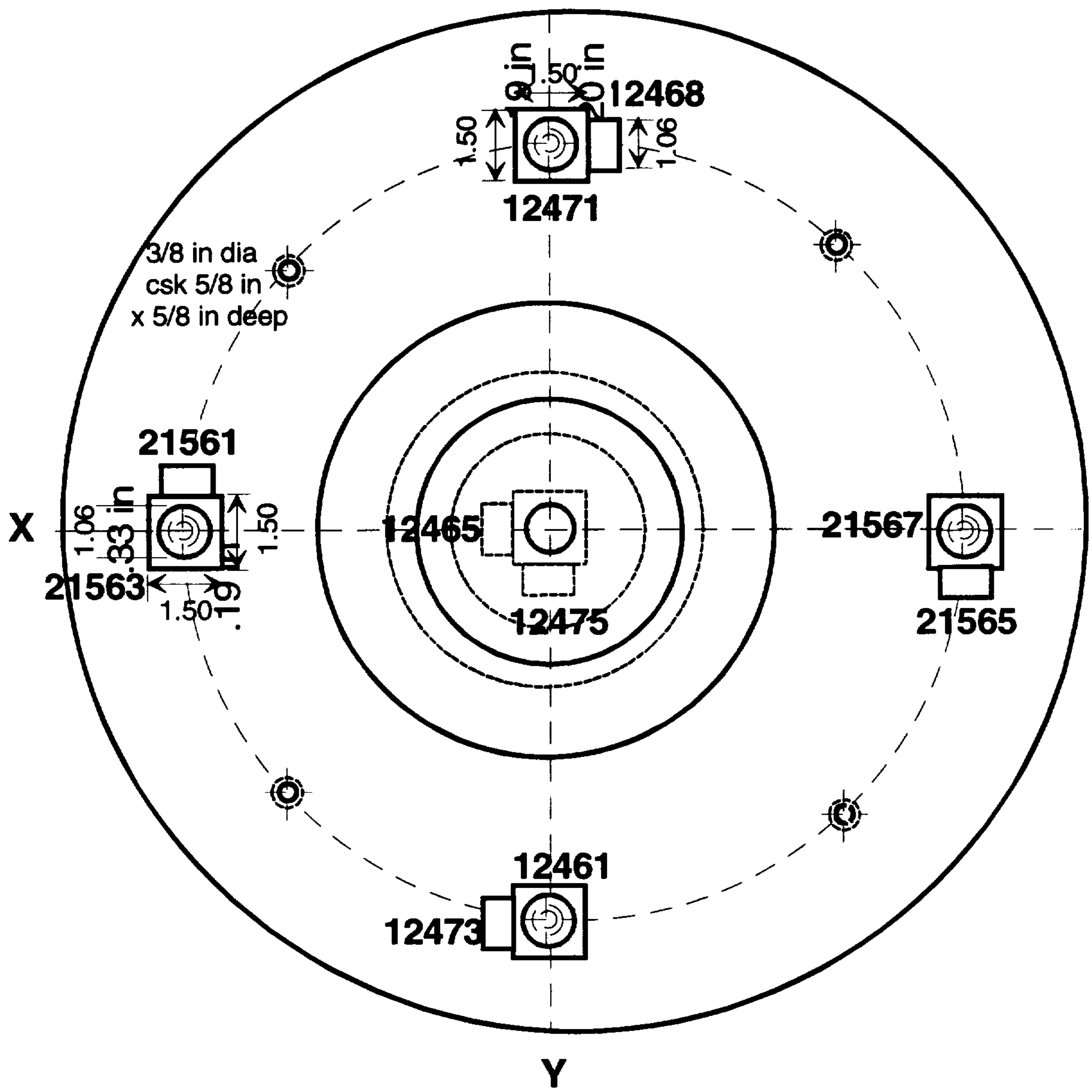

Figure 2. - Detailed Drawing of Test Apparatus Platform with Accelerometers
a. TOP View - XY Plane

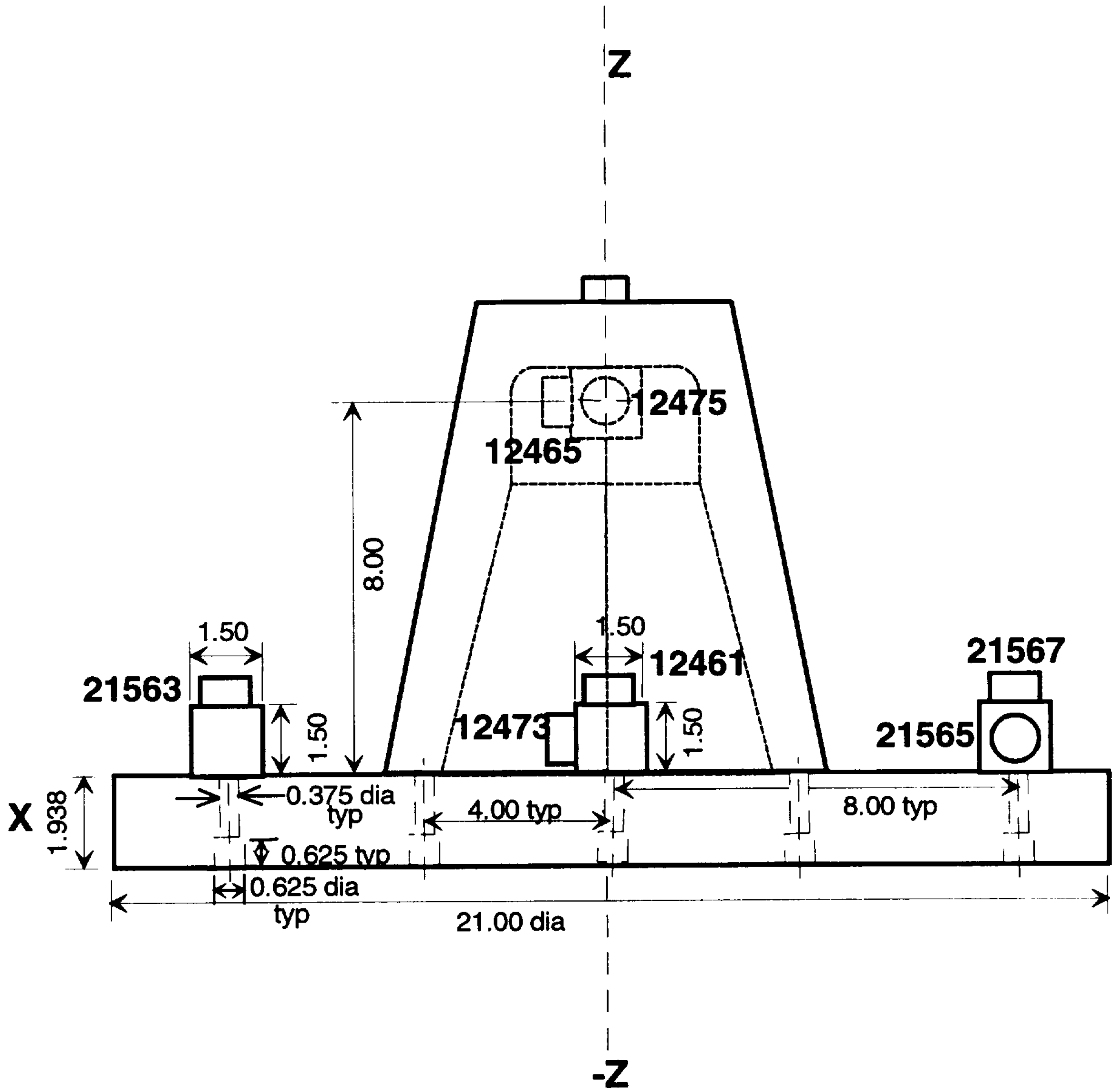

Figure 2. - Detailed Drawing of Test Apparatus Platform with Accelerometers
b. Side View - XZ Plane

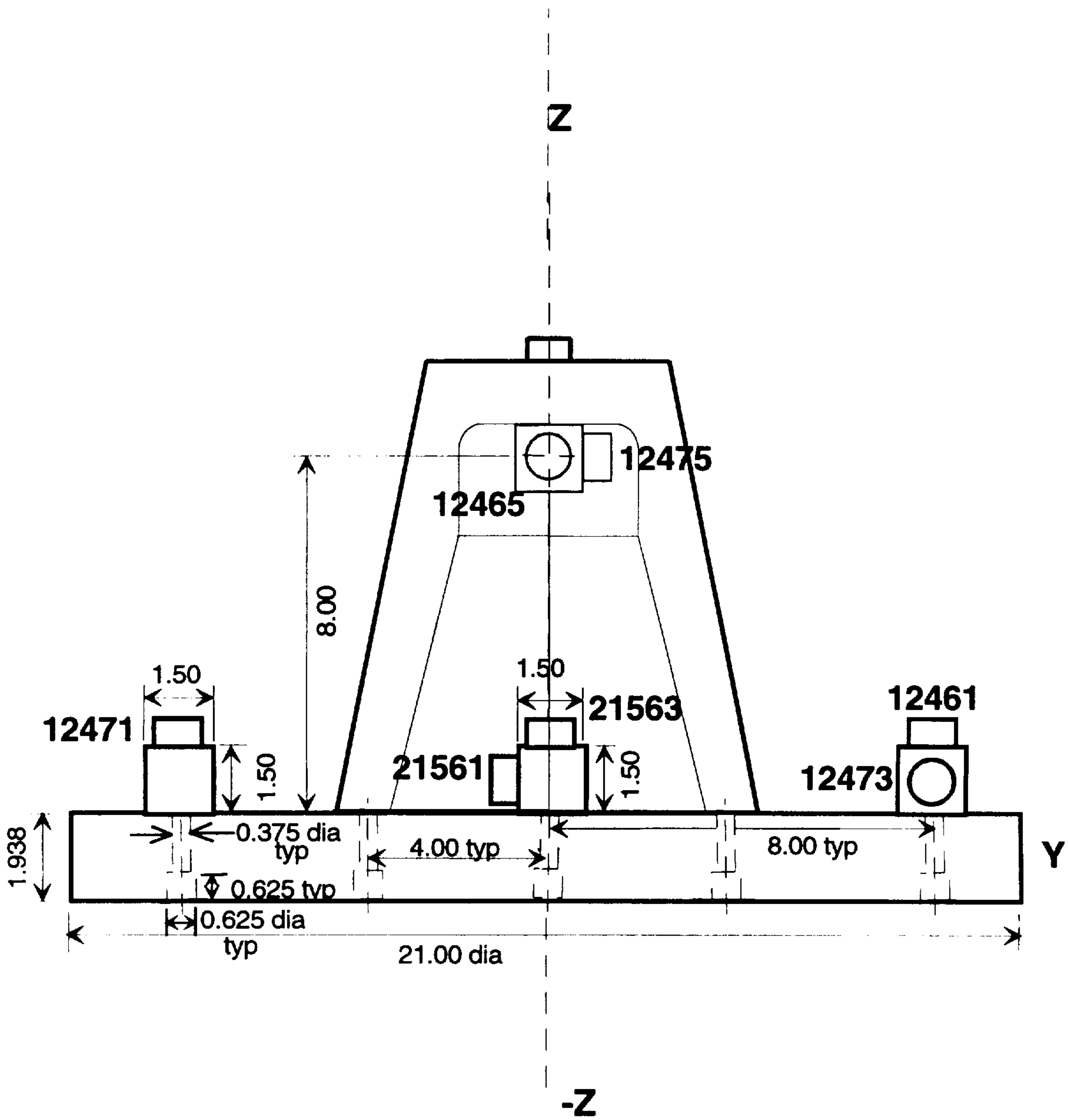

Figure 2. - Detailed Drawing of Test Apparatus Platform with Accelerometers
c. Side View - YZ Plane

Apparatus weight	98.4	Lb
Circular plate		
Diameter	21	in
Thickness	2.0	in
Cone		
Height	10	in
Thickness	1.5	in
Base Dia.	9.5	in
Tip Dia.	5.5	in

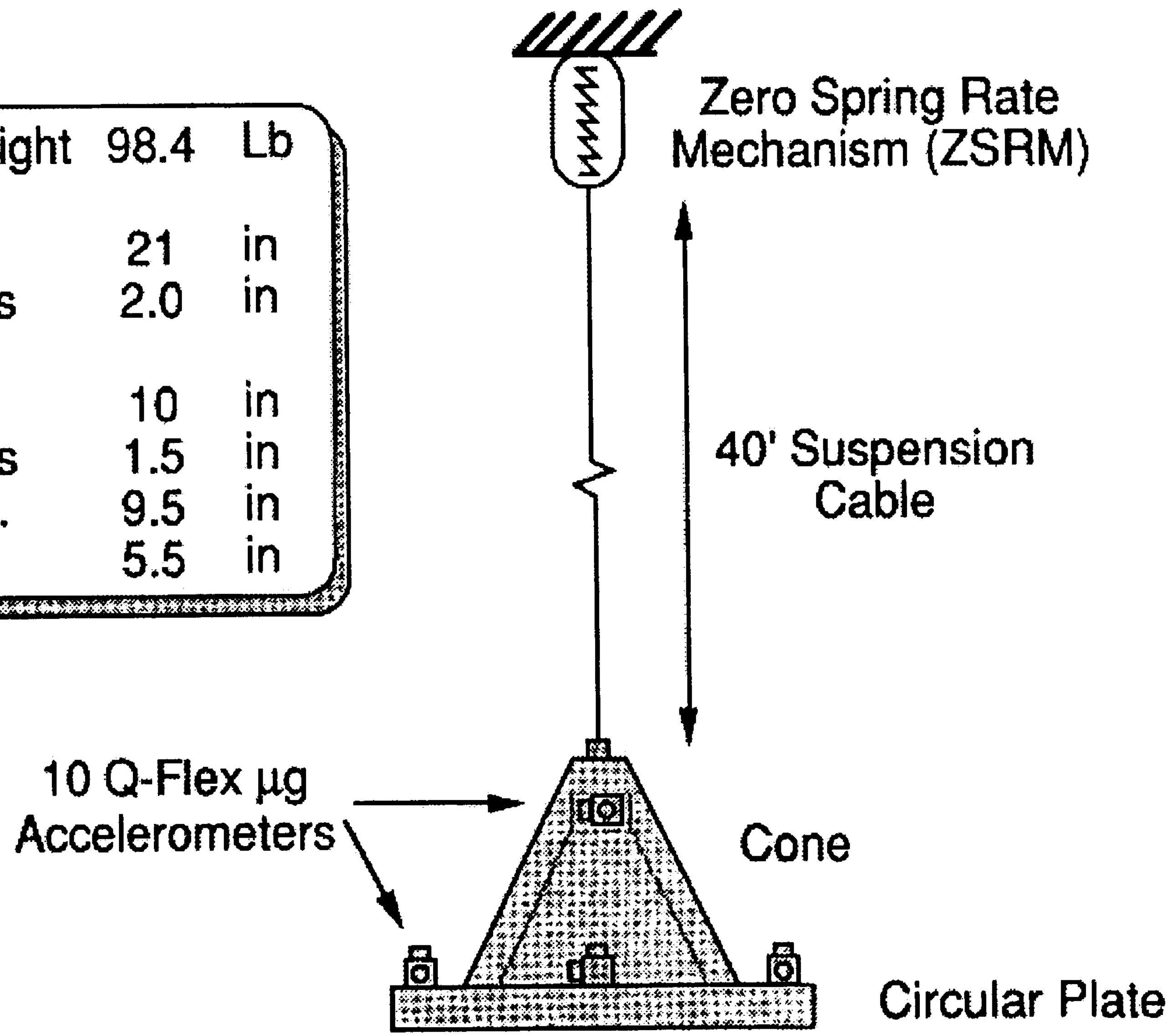

Figure 3.- Schematic of Test Apparatus with Suspension System

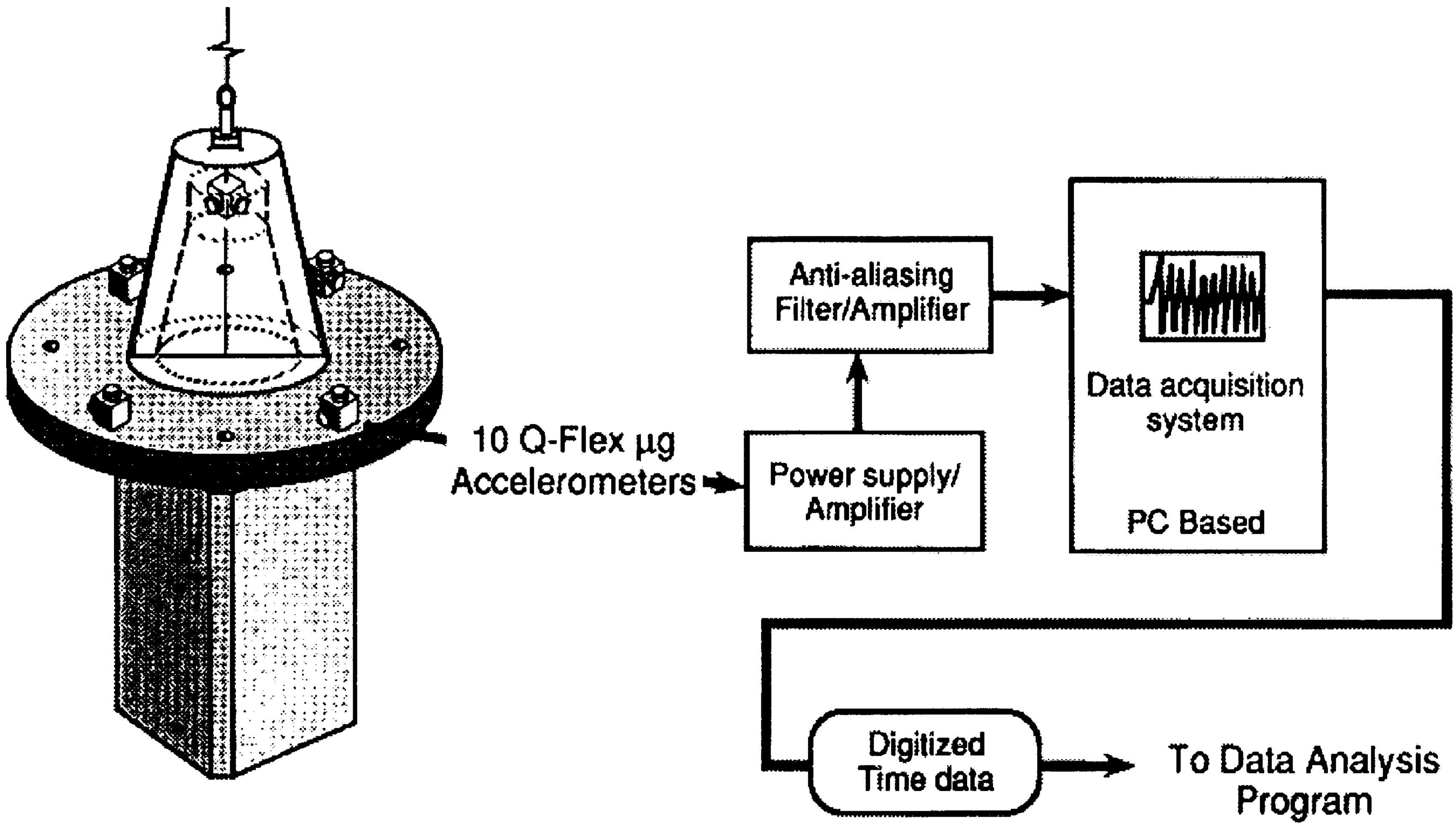

Figure 4. - Data Acquisition System

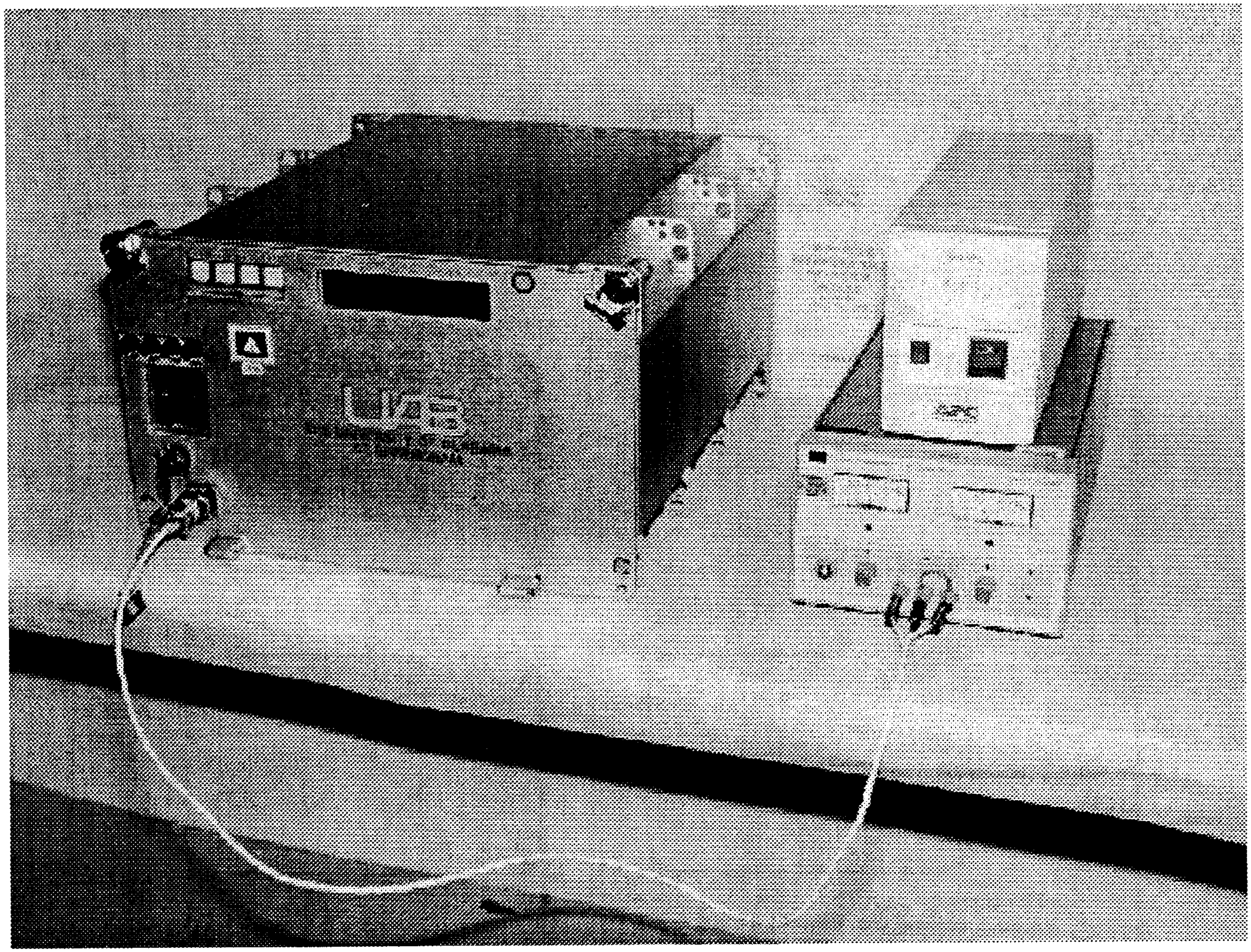

Figure 5. - Commercial Refrigeration/ Incubation Module

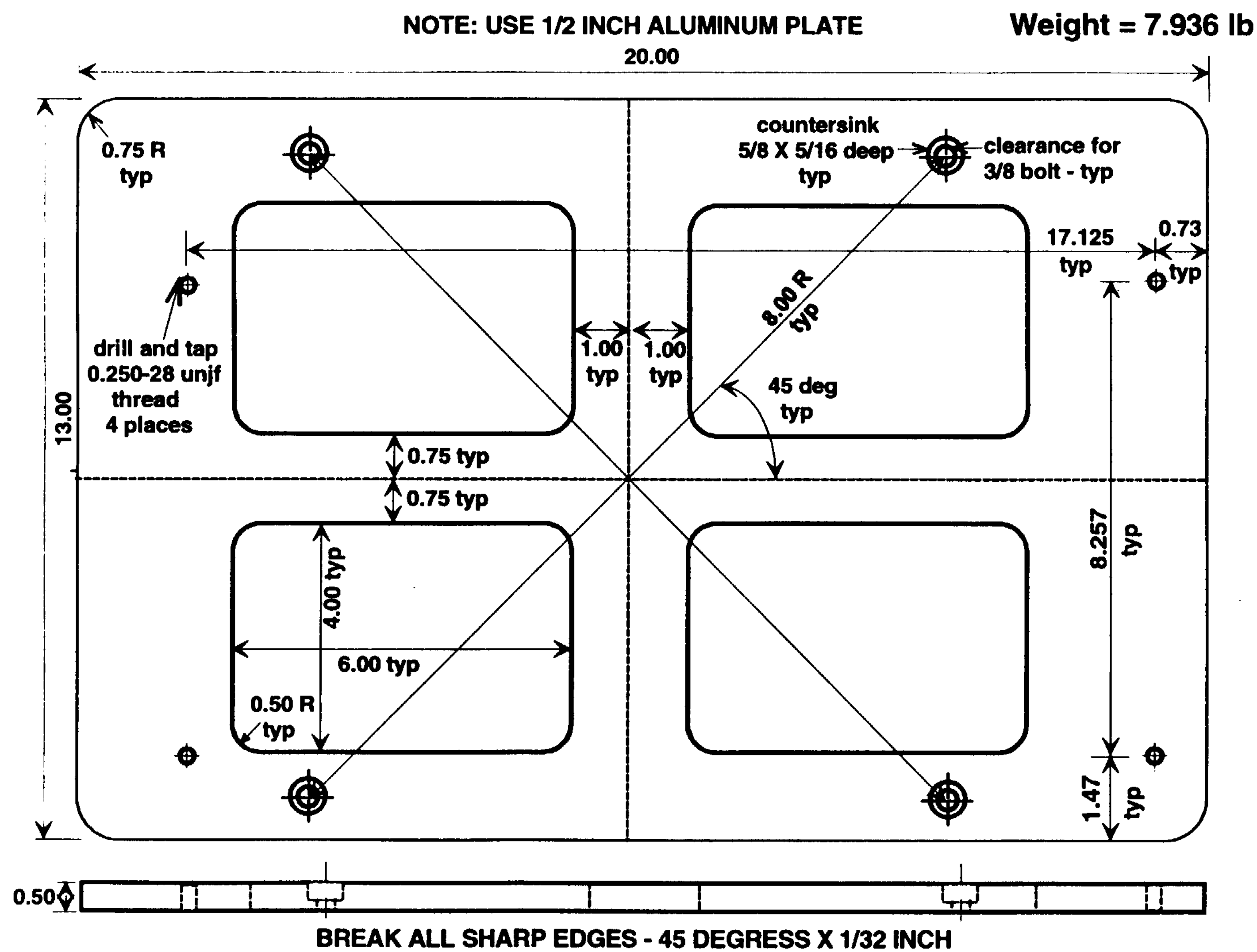

Figure 6. - CRIM Interface Plate

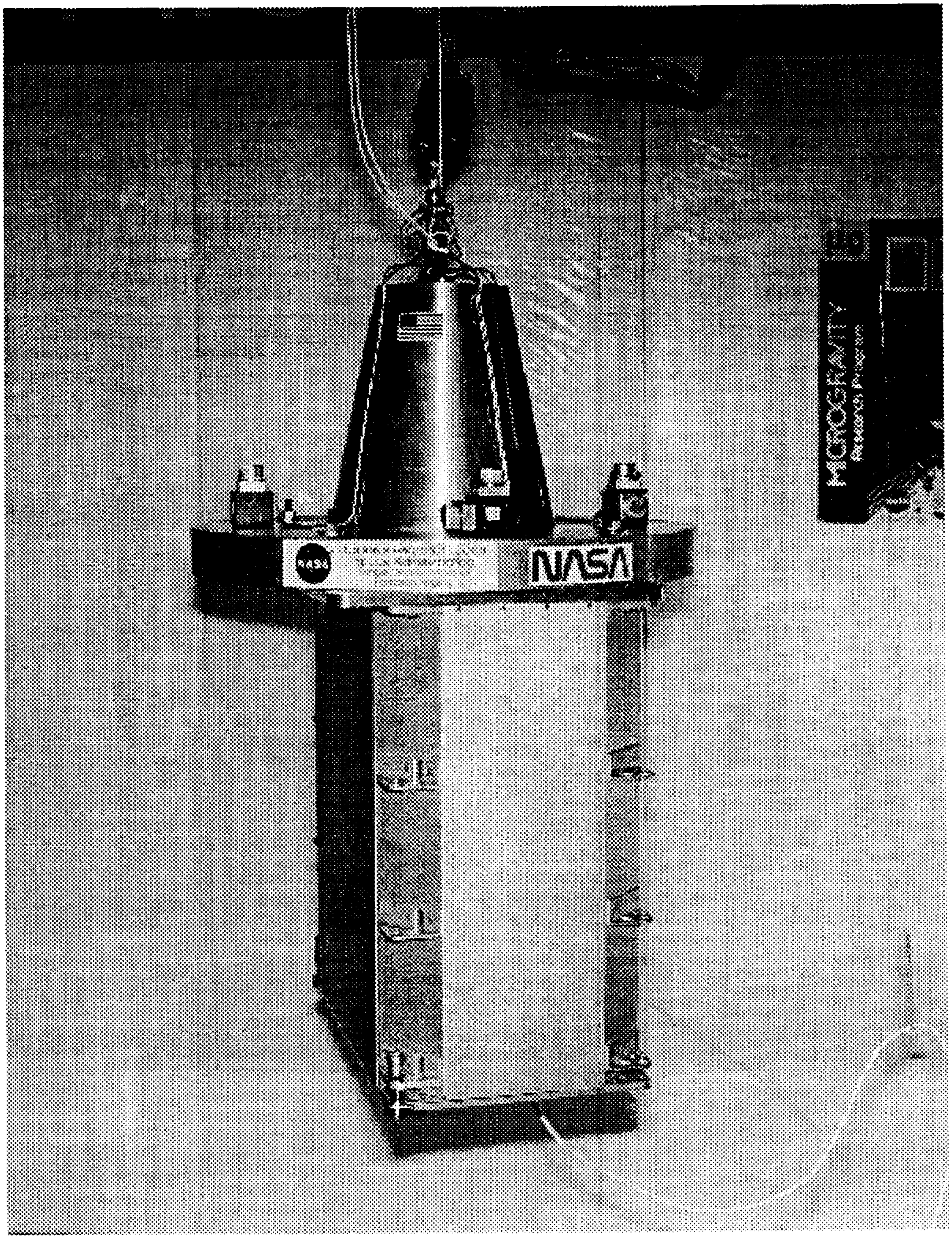

Figure 7. - Installation of CRIM on Test Apparatus Platform

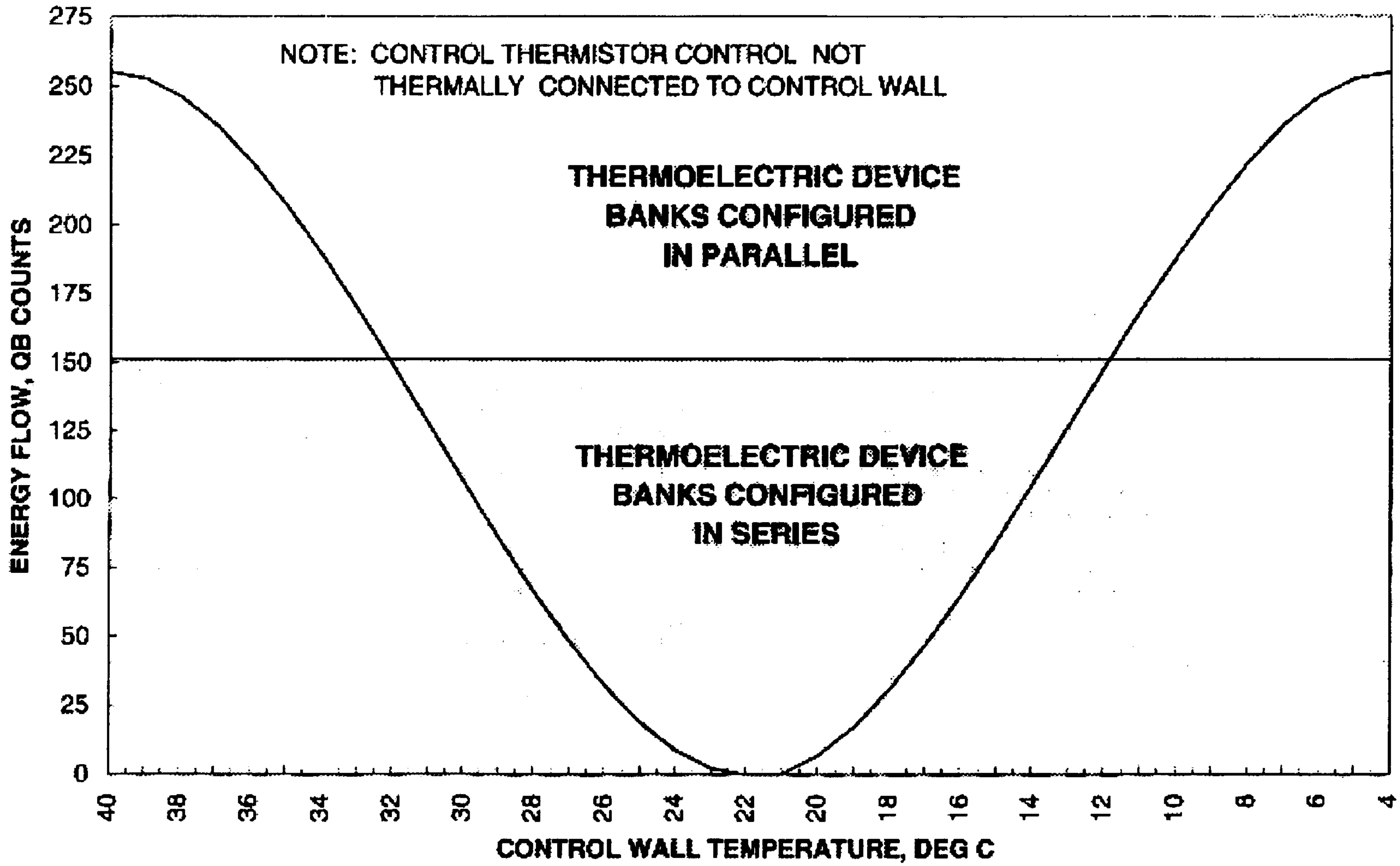

Figure 8. - Variation of Energy Flow with Control Wall Temperature

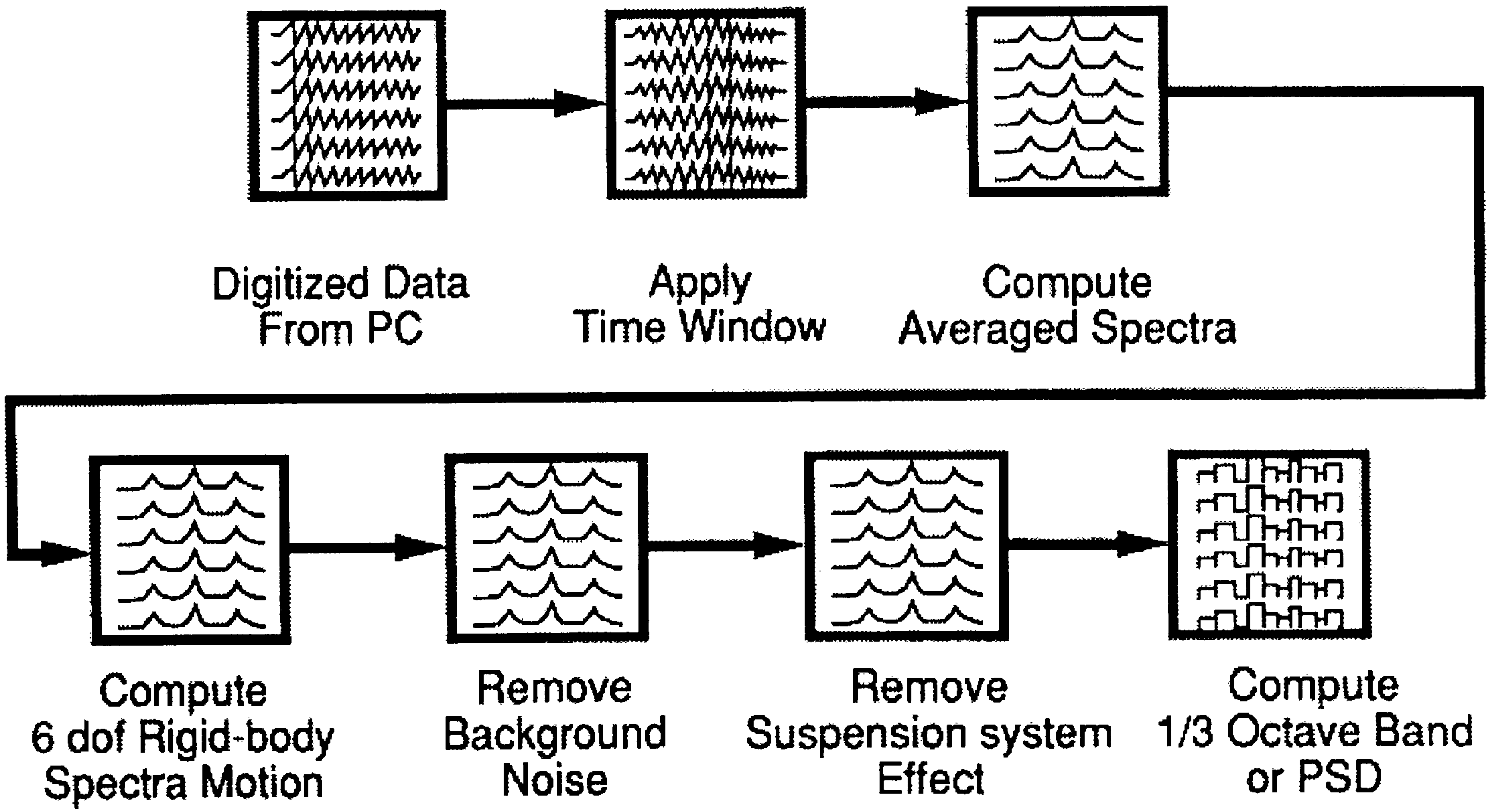

Figure 9. - Data Analysis Process

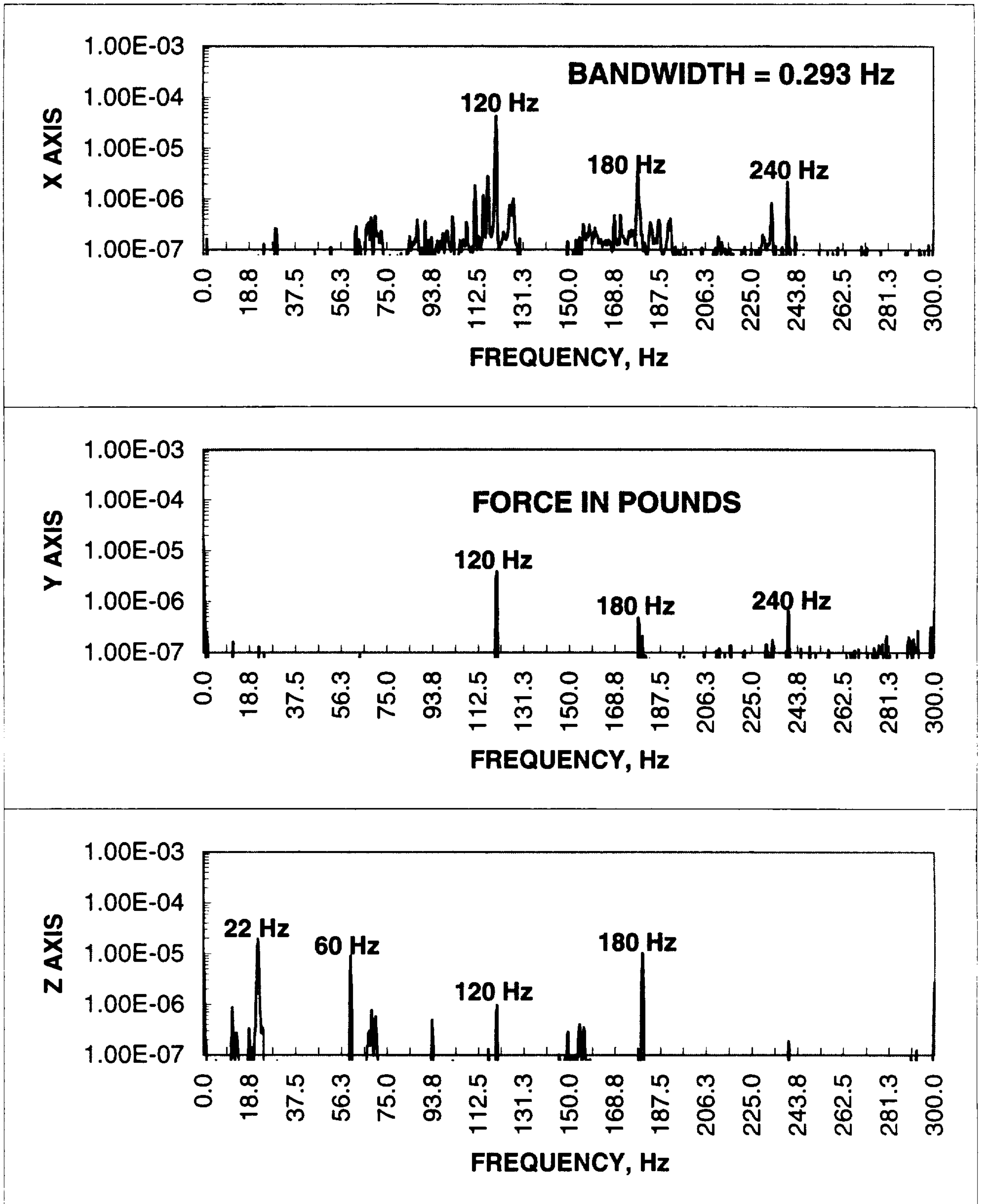

Figure 10. - Background Force Power Spectral Density - Test Point 31

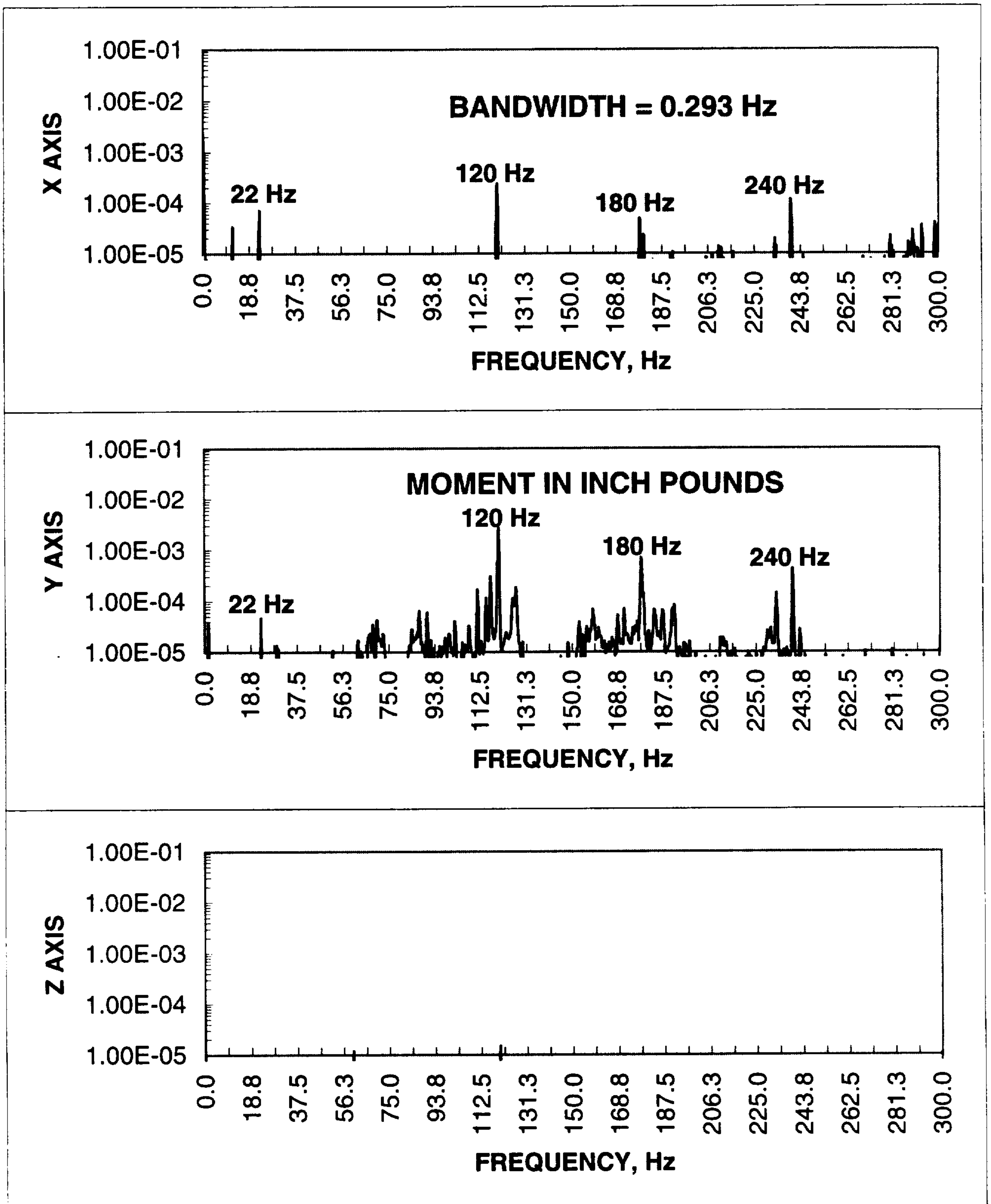

Figure 11. - Background Moment Power Spectral Density - Test Point 31

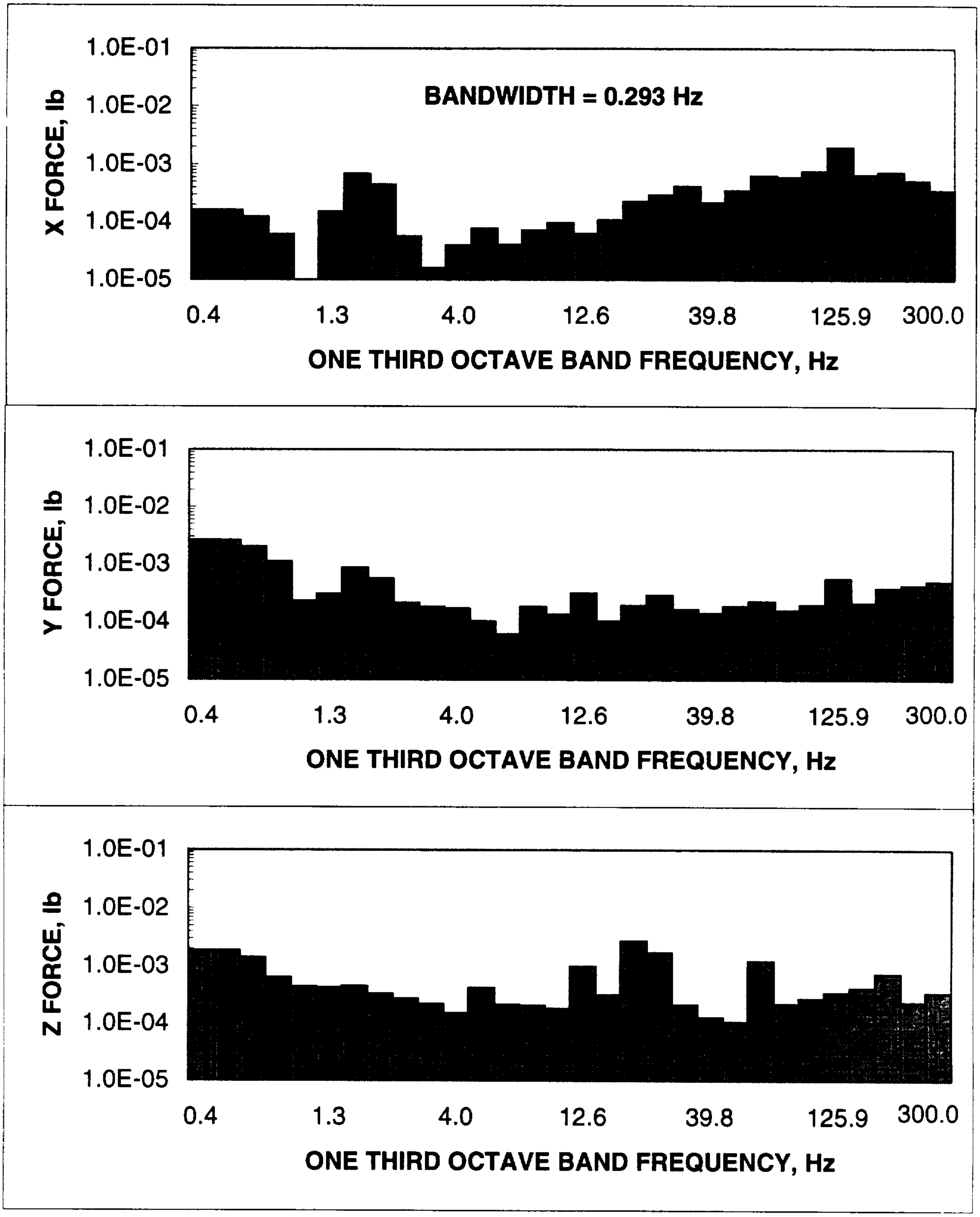

Figure 12. - Background One Third Octave Band Force - Test Point 31

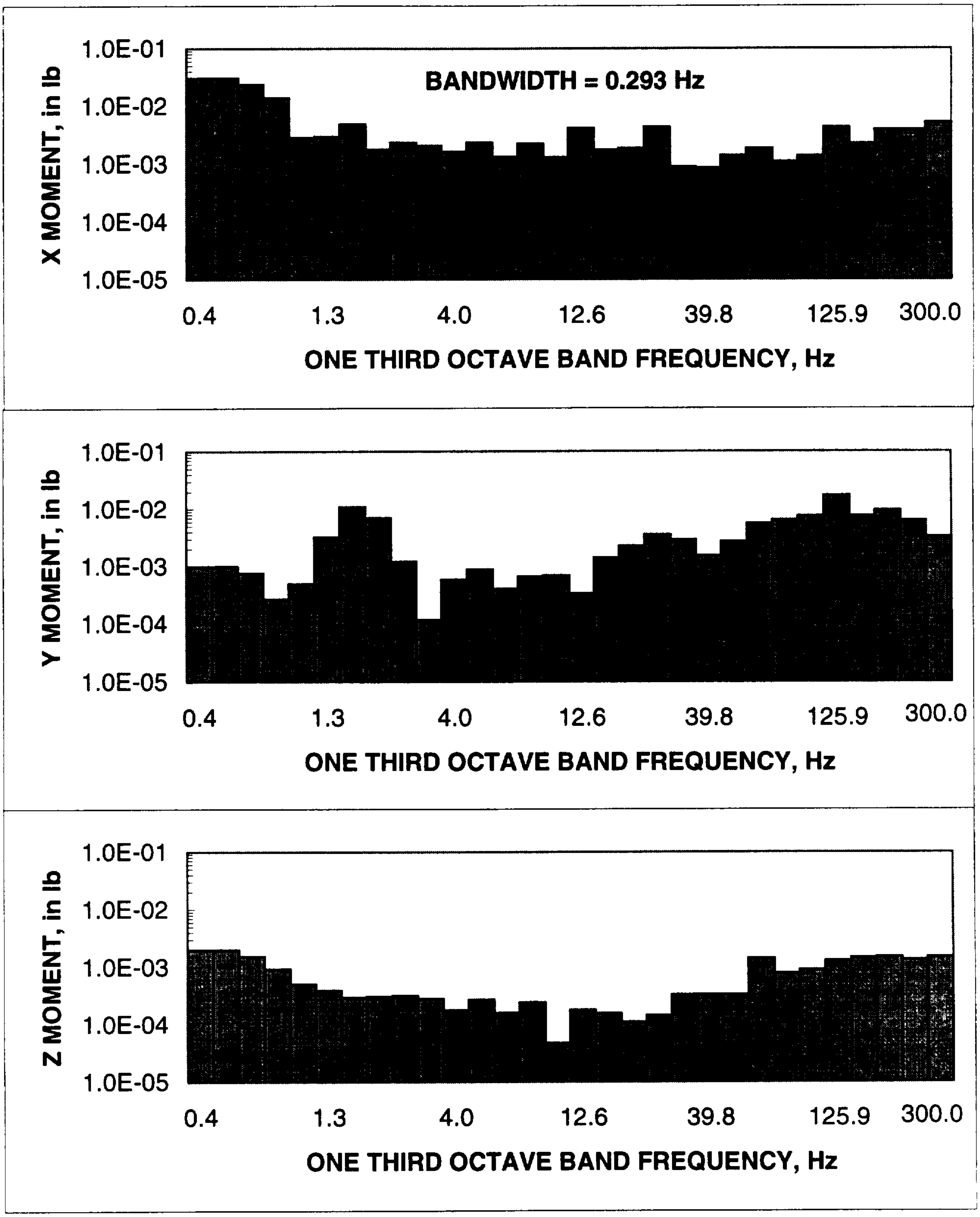

Figure 13. - Background One Third Octave Band Moment - Test Point 31

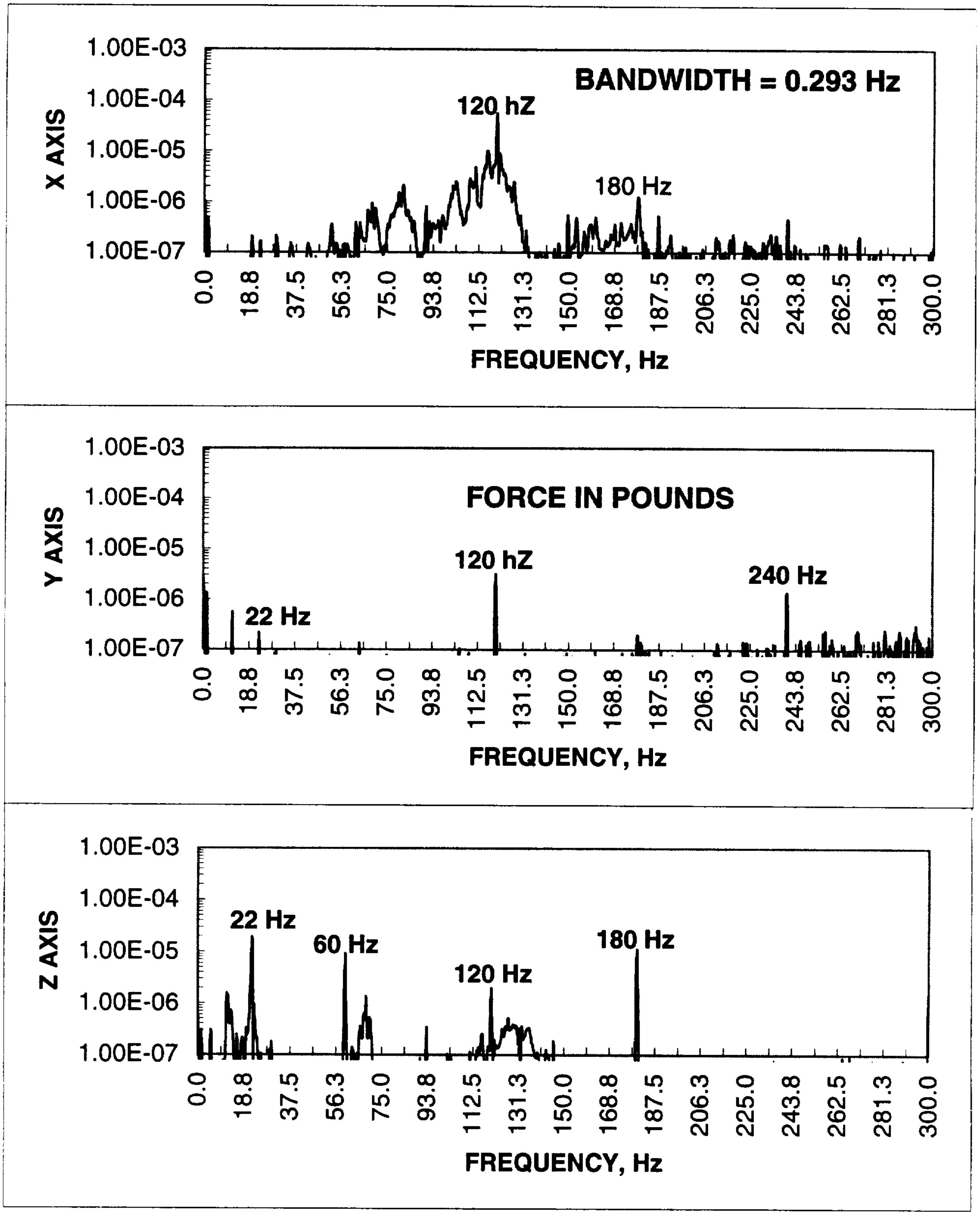

Figure 14. - Background Force Power Spectral Density - Test Point 65

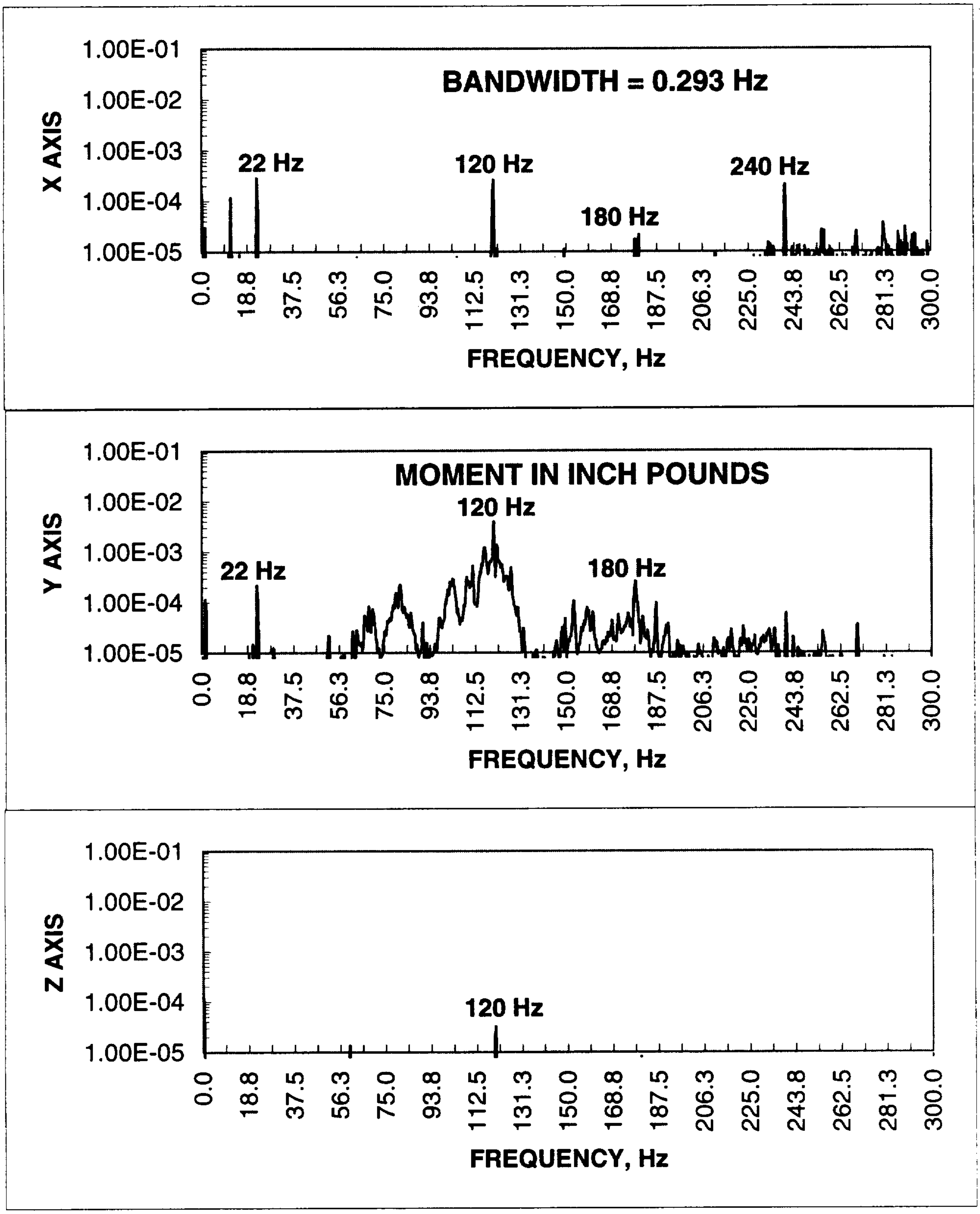

Figure 15. - Background Moment Power Spectral Density - Test Point 65

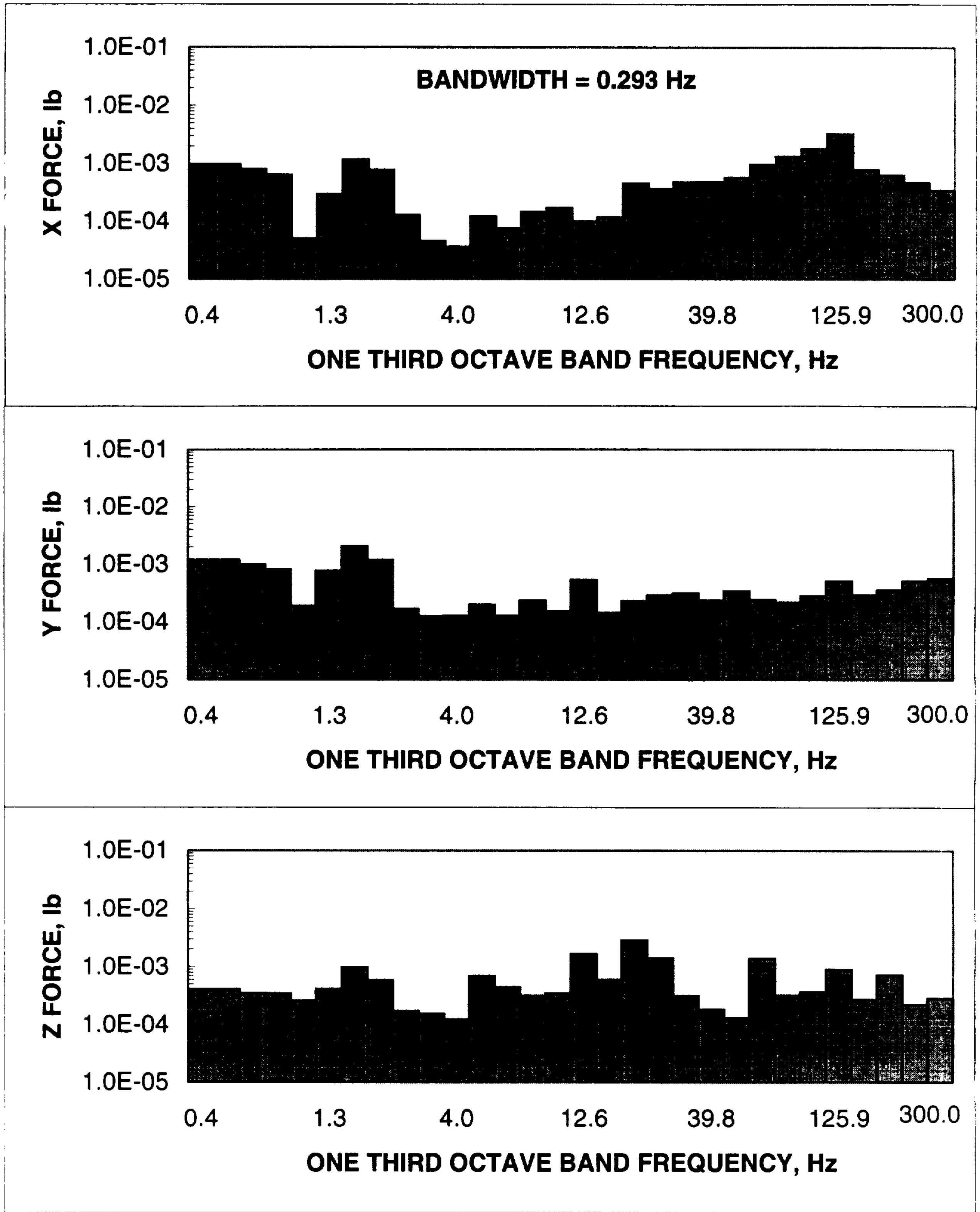

Figure 16. - Background One Third Octave Band Force - Test Point 65

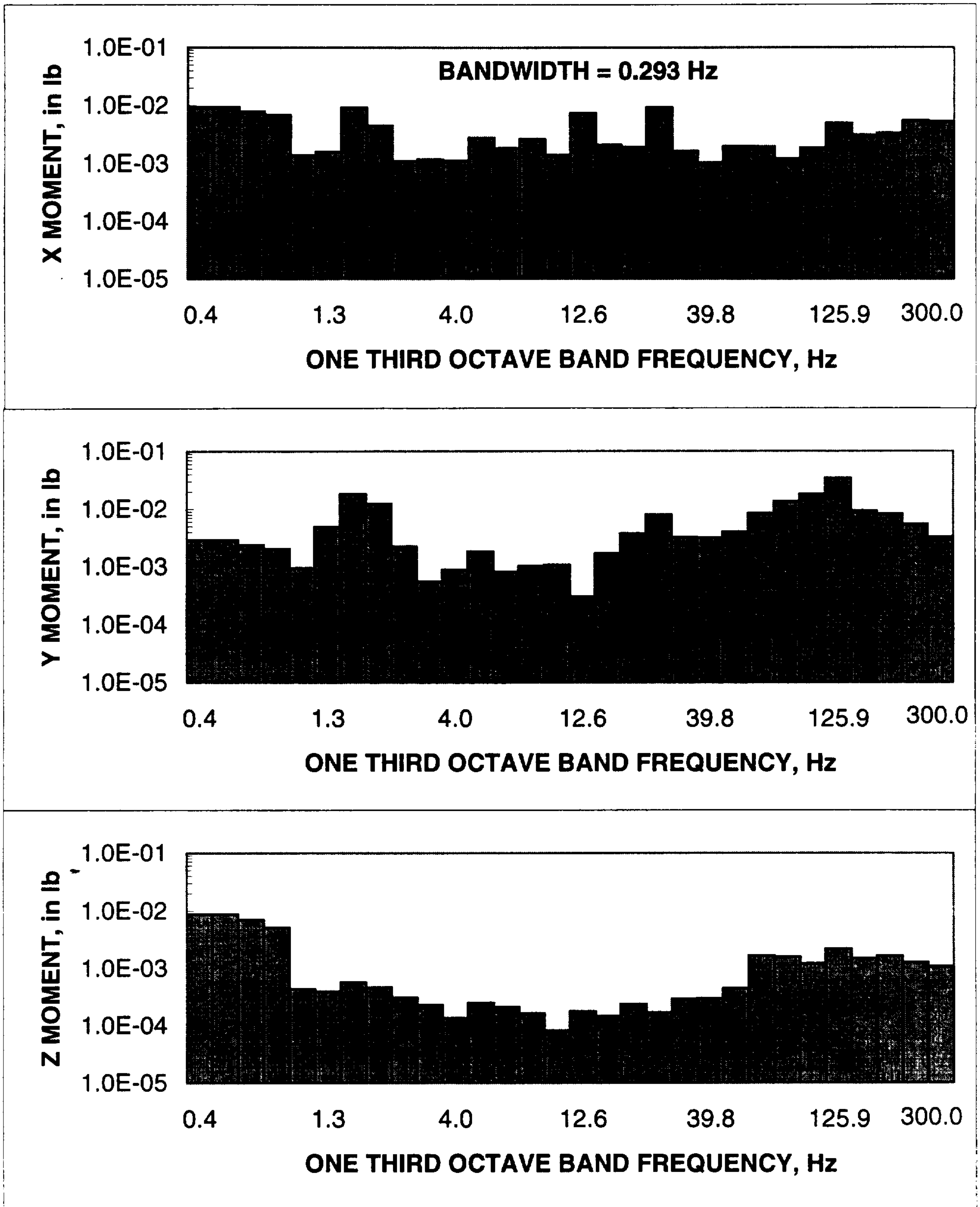

Figure 17. - Background One Third Octave Band Moment - Test Point 65

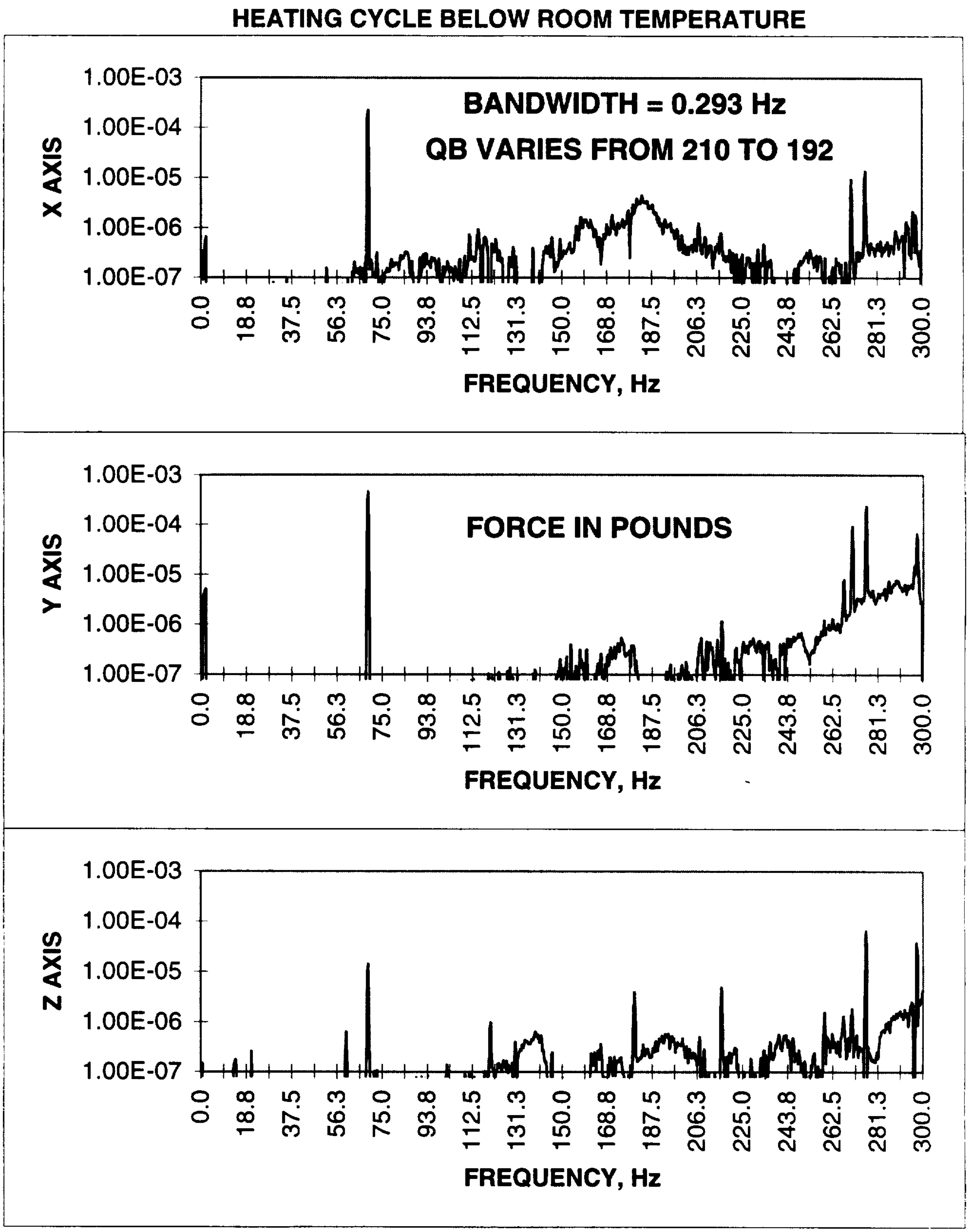

Figure 18. - CRIM Force Power Spectral Density - Test Point 38

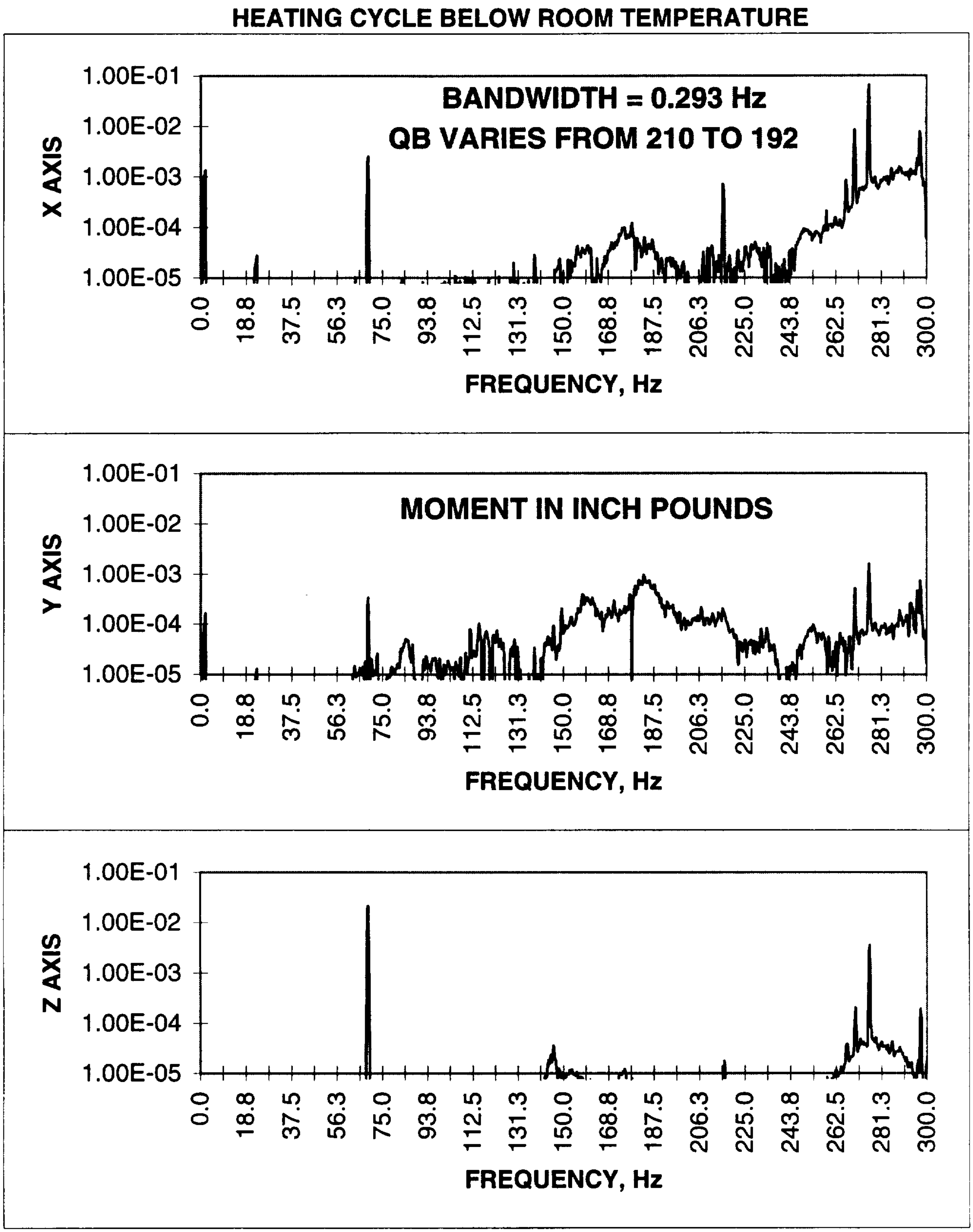

Figure 19. - CRIM Moment Power Spectral Density - Test Point 38

HEATING CYCLE BELOW ROOM TEMPERATURE

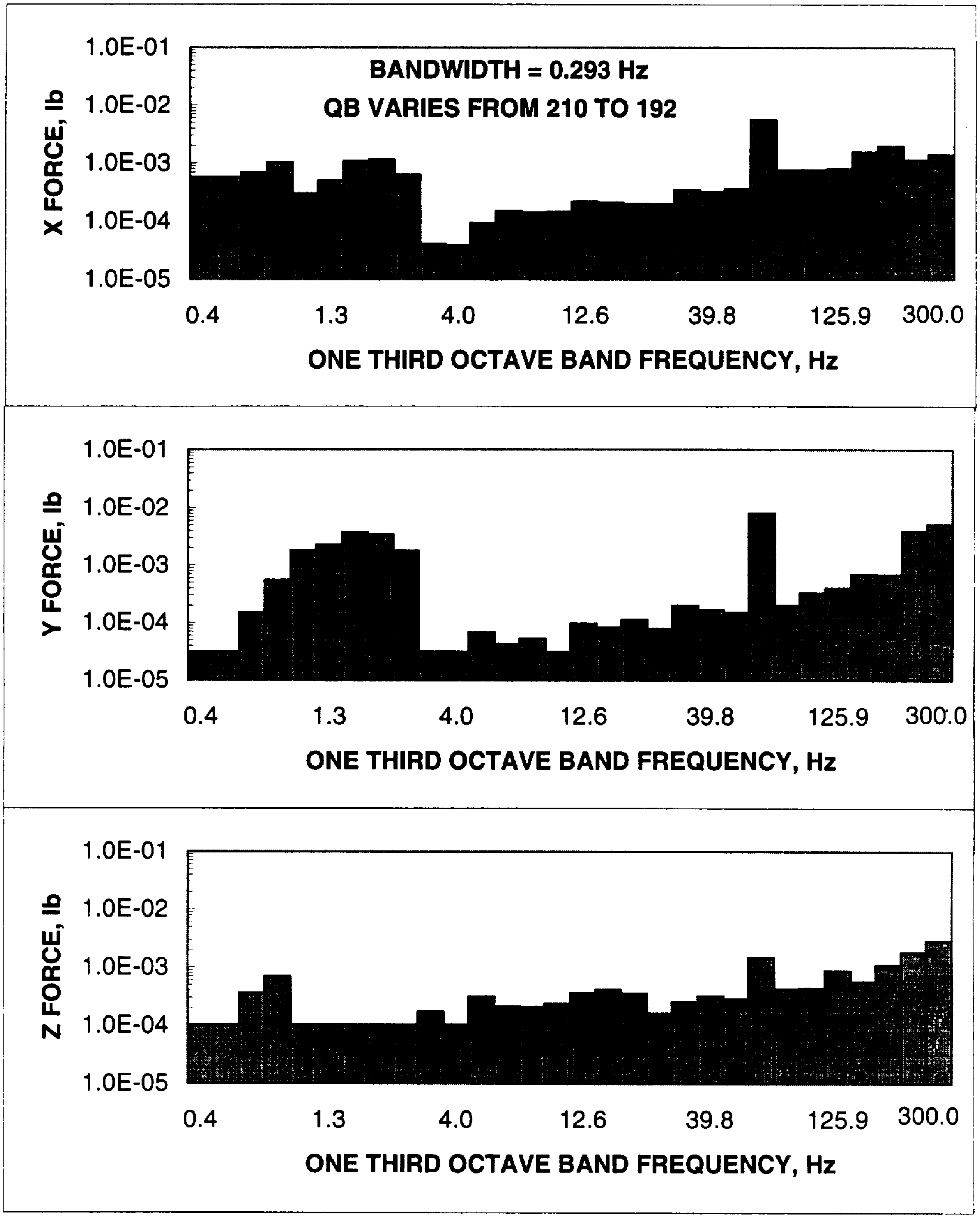

Figure 20. - CRIM One Third Octave Band Force - Test Point 38

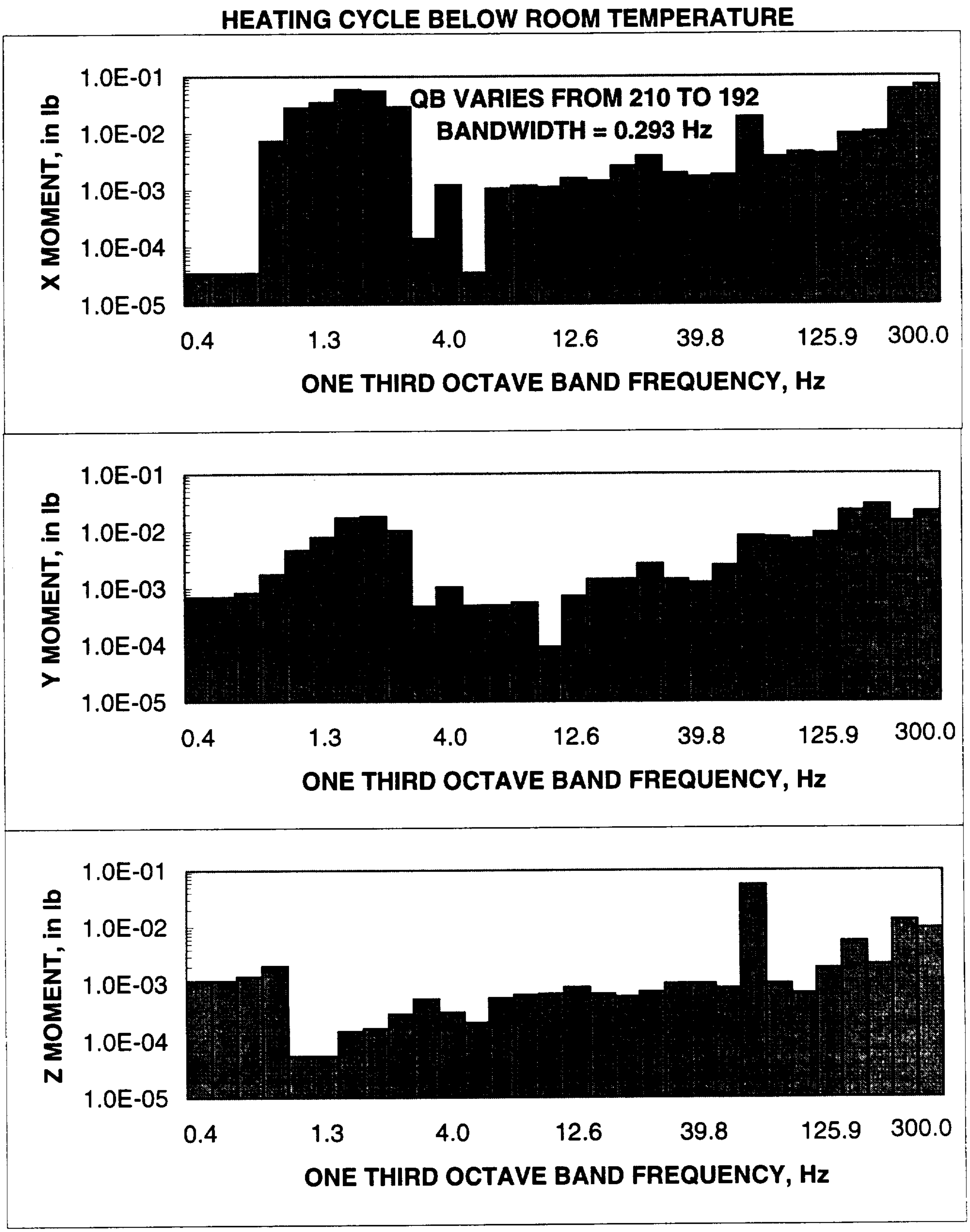

Figure 21. - CRIM One Third Octave Band Moment - Test Point 38

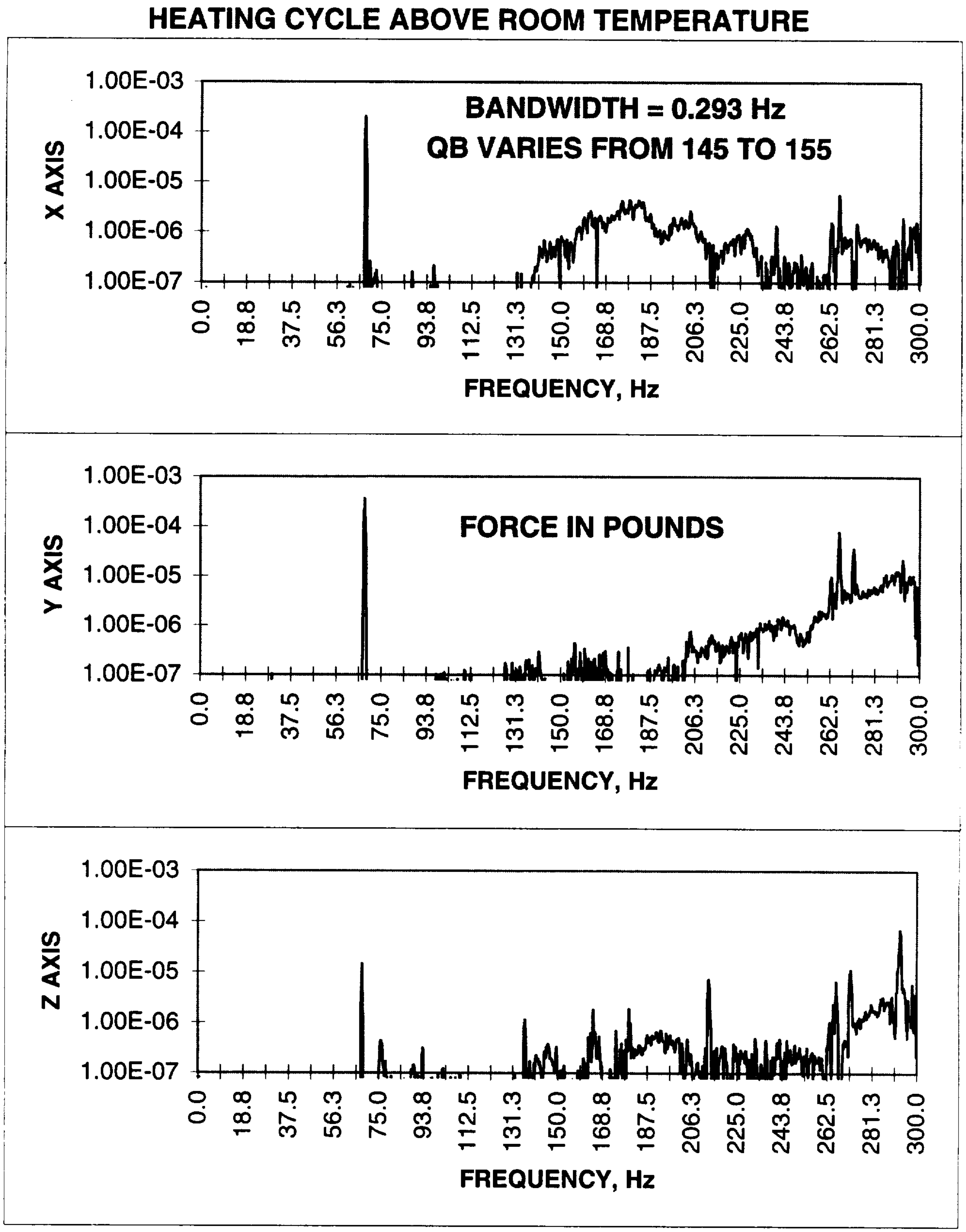

Figure 22. - CRIM Force Power Spectral Density - Test Point 51

HEATING CYCLE ABOVE ROOM TEMPERATURE

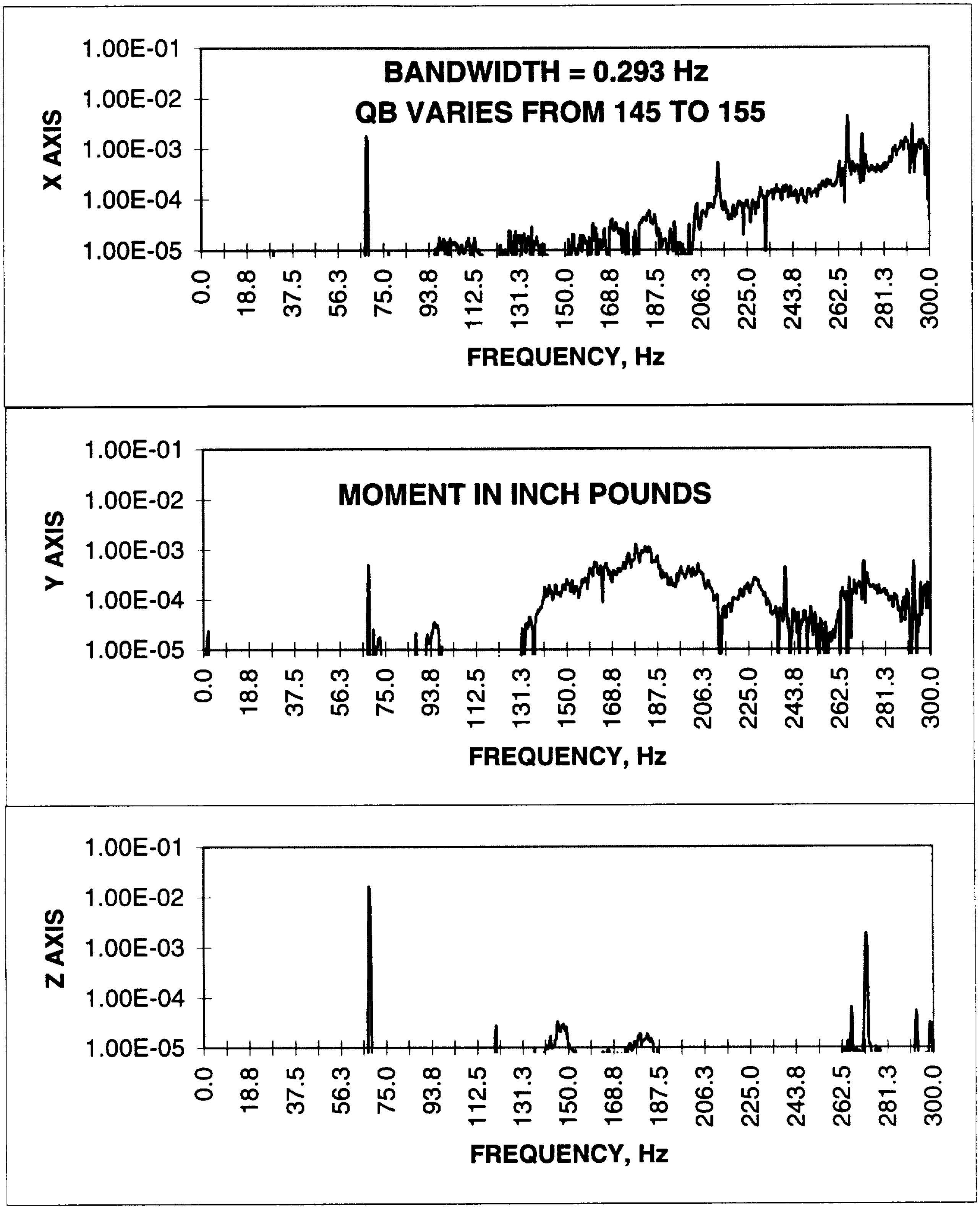

Figure 23. - CRIM Moment Power Spectral Density - Test Point 51

HEATING CYCLE ABOVE ROOM TEMPERATURE

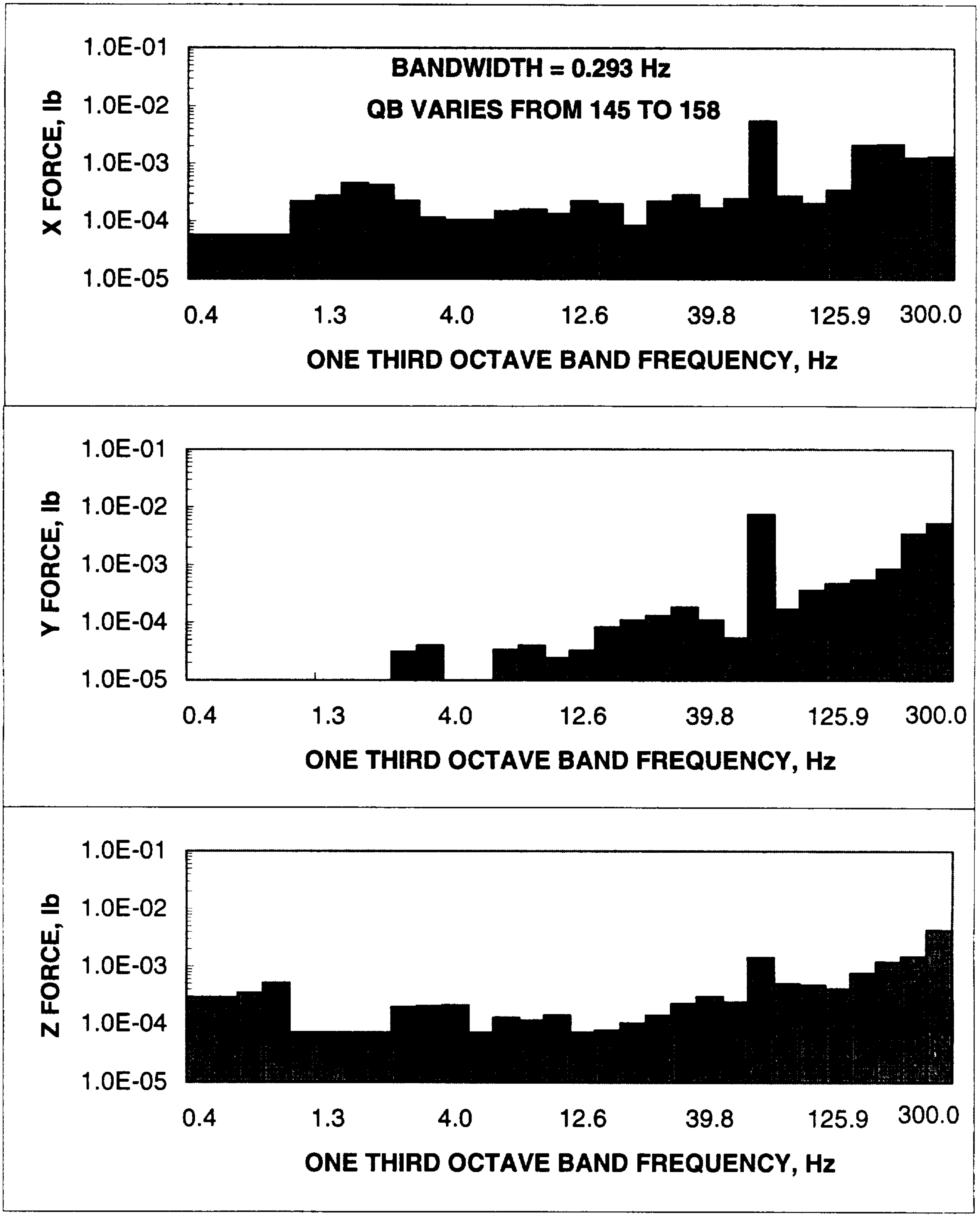

Figure 24. - CRIM One Third Octave Band Force - Test Point 51

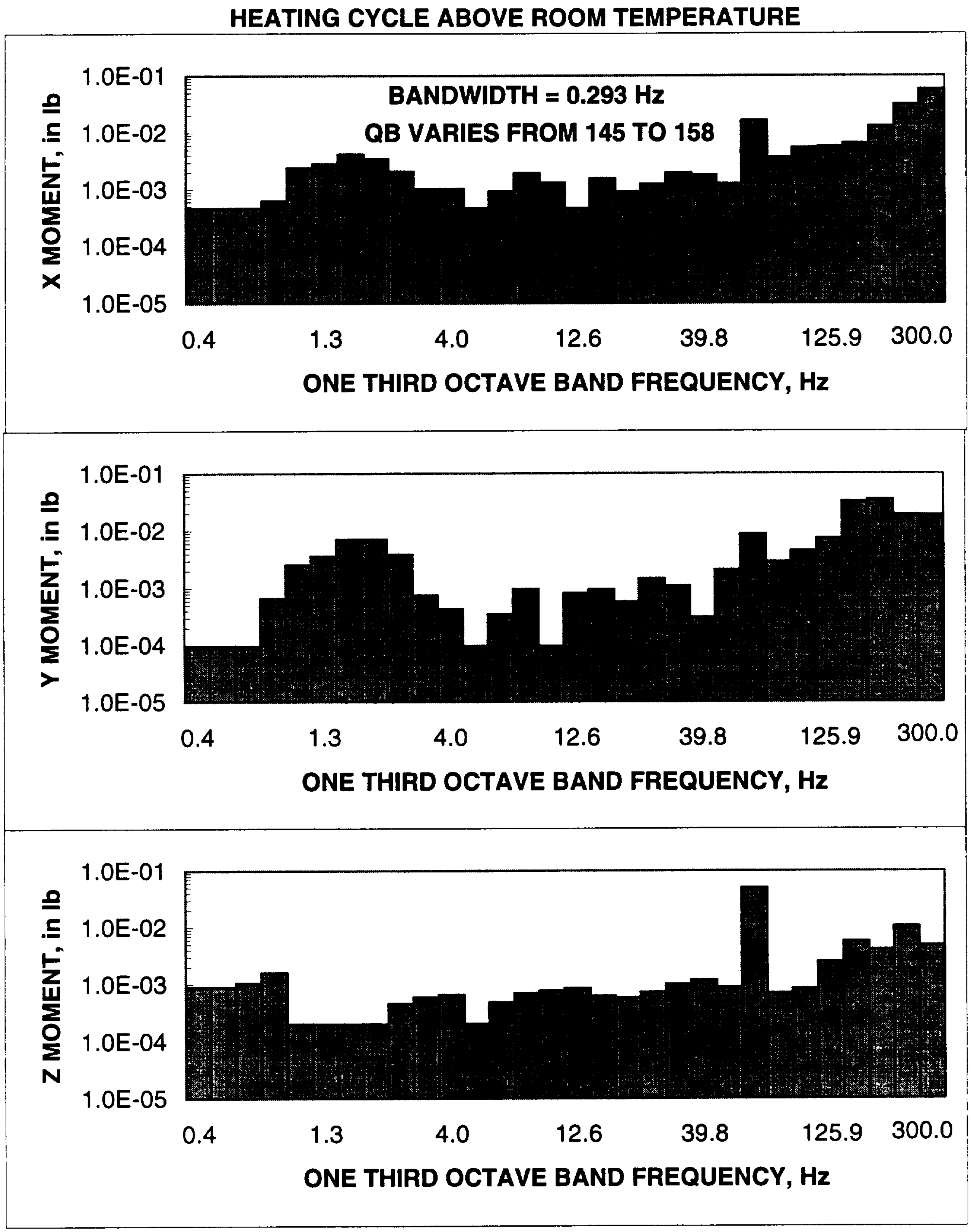

Figure 25. - CRIM One Third Octave Band Moment - Test Point 51

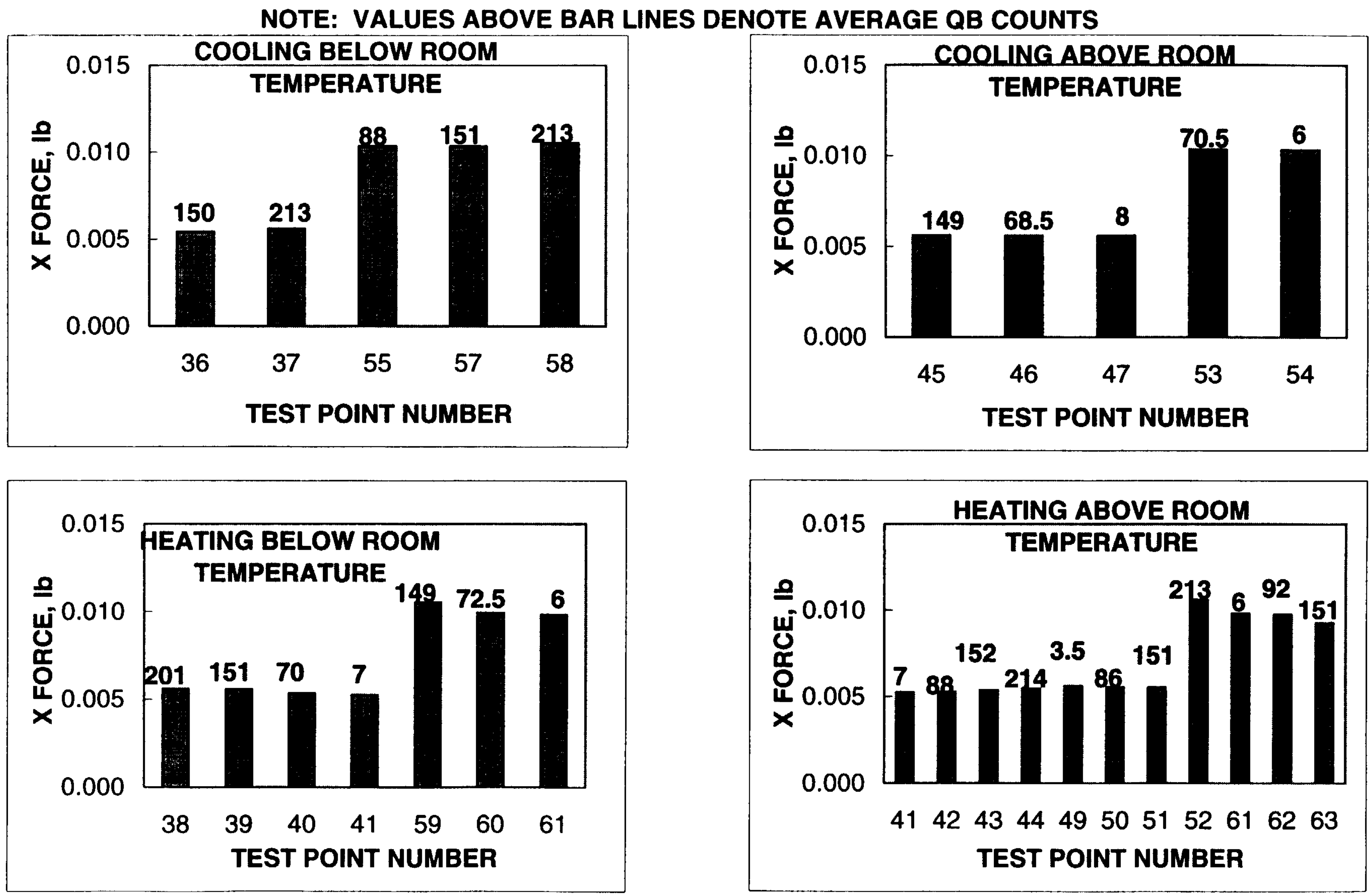

Figure 26. - X Force - One Third Octave Center Band Frequency = 63 Hz

NOTE: VALUES ABOVE BAR LINES DENOTE AVERAGE QB COUNTS

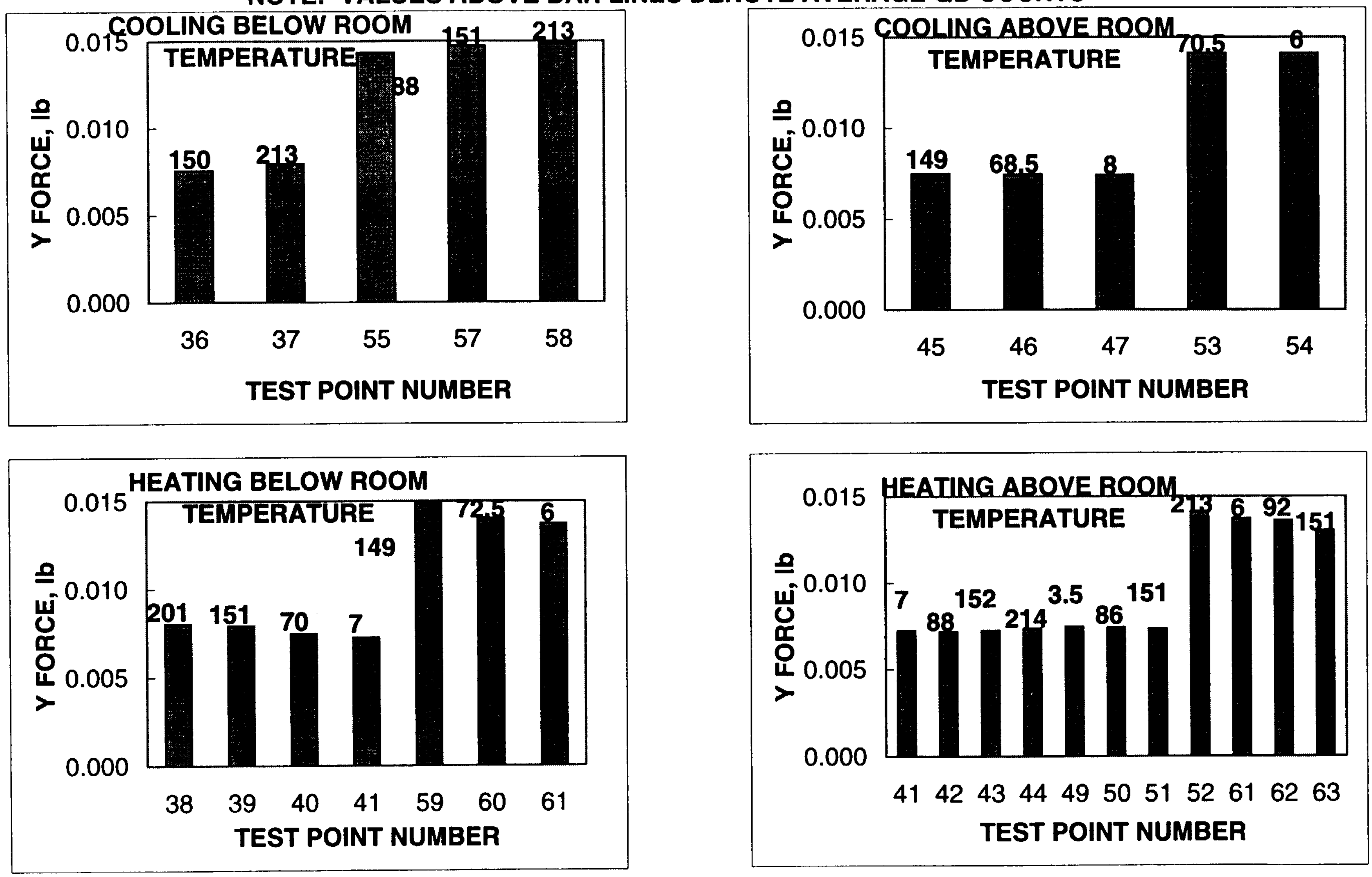

Figure 27. - Y Force - One Third Octave Center Band Frequency = 63 Hz

NOTE: VALUES ABOVE BAR LINES DENOTE AVERAGE QB COUNTS

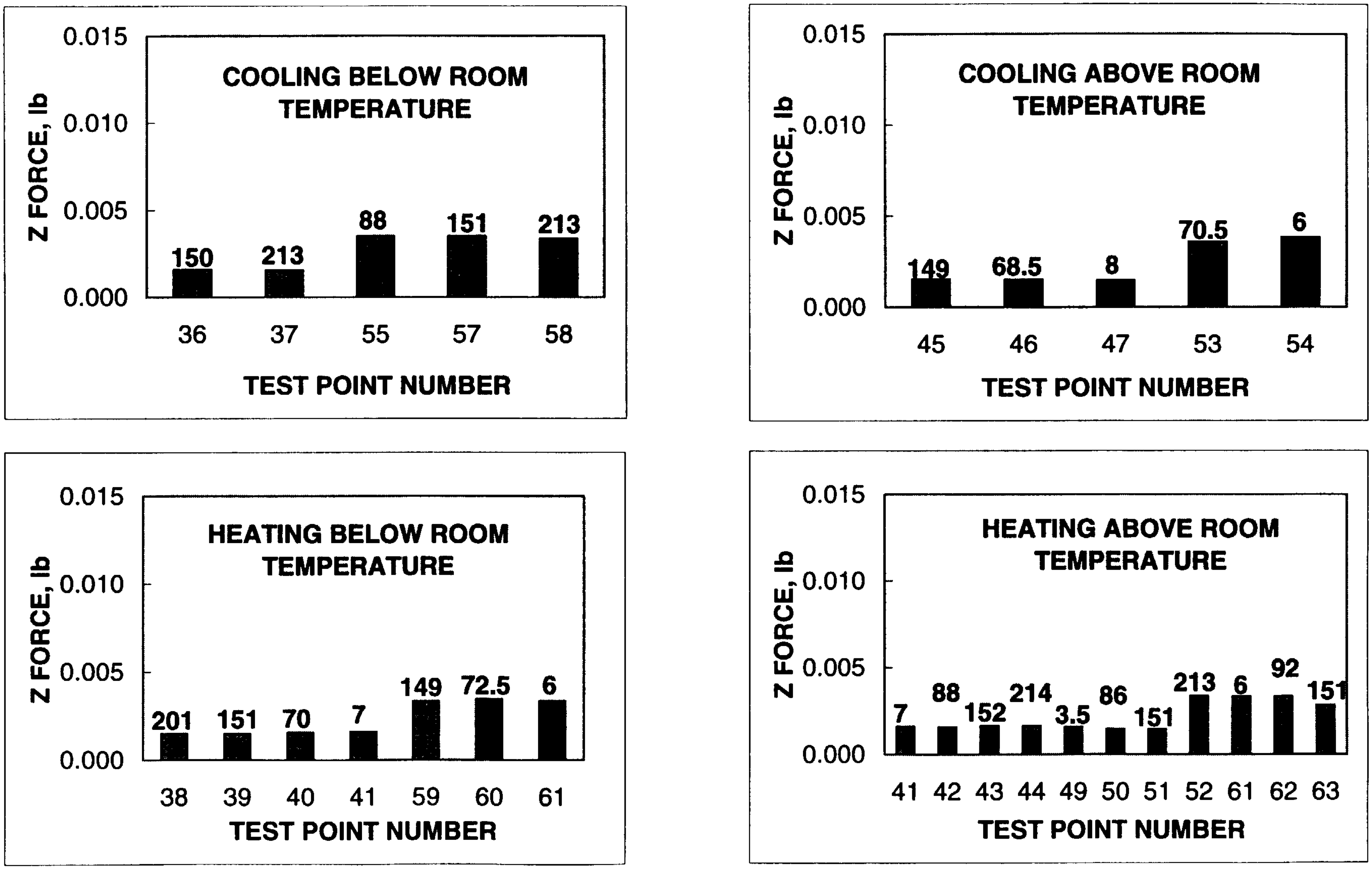

Figure 28. - Z Force - One Third Octave Center Band Frequency = 63 Hz

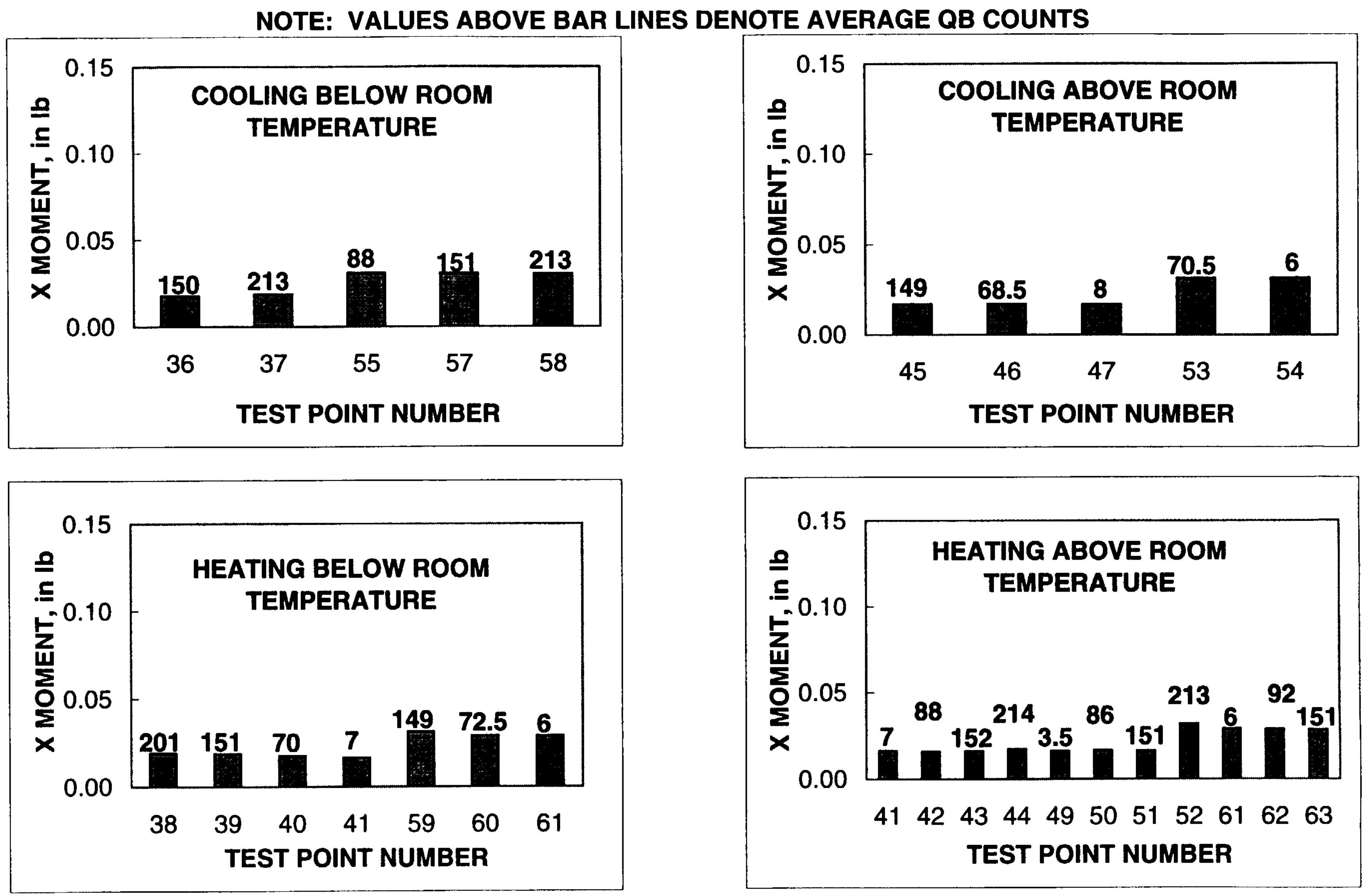

Figure 29. - X Moment - One Third Octave Center Band Frequency = 63 Hz

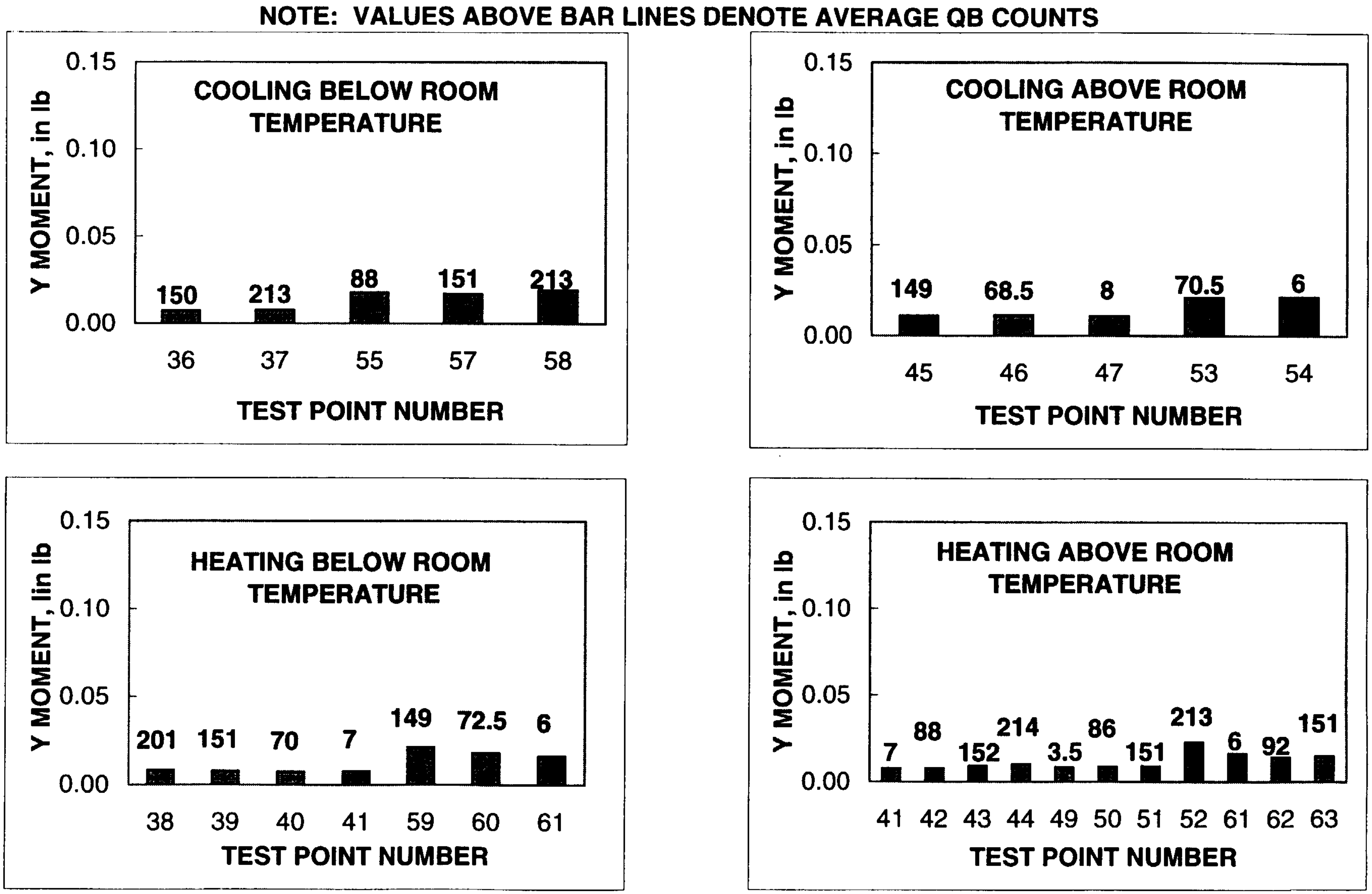

Figure 30. - Y Moment - One Third Octave Center Band Frequency = 63 Hz

NOTE: VALUES ABOVE BAR LINES DENOTE AVERAGE QB COUNTS

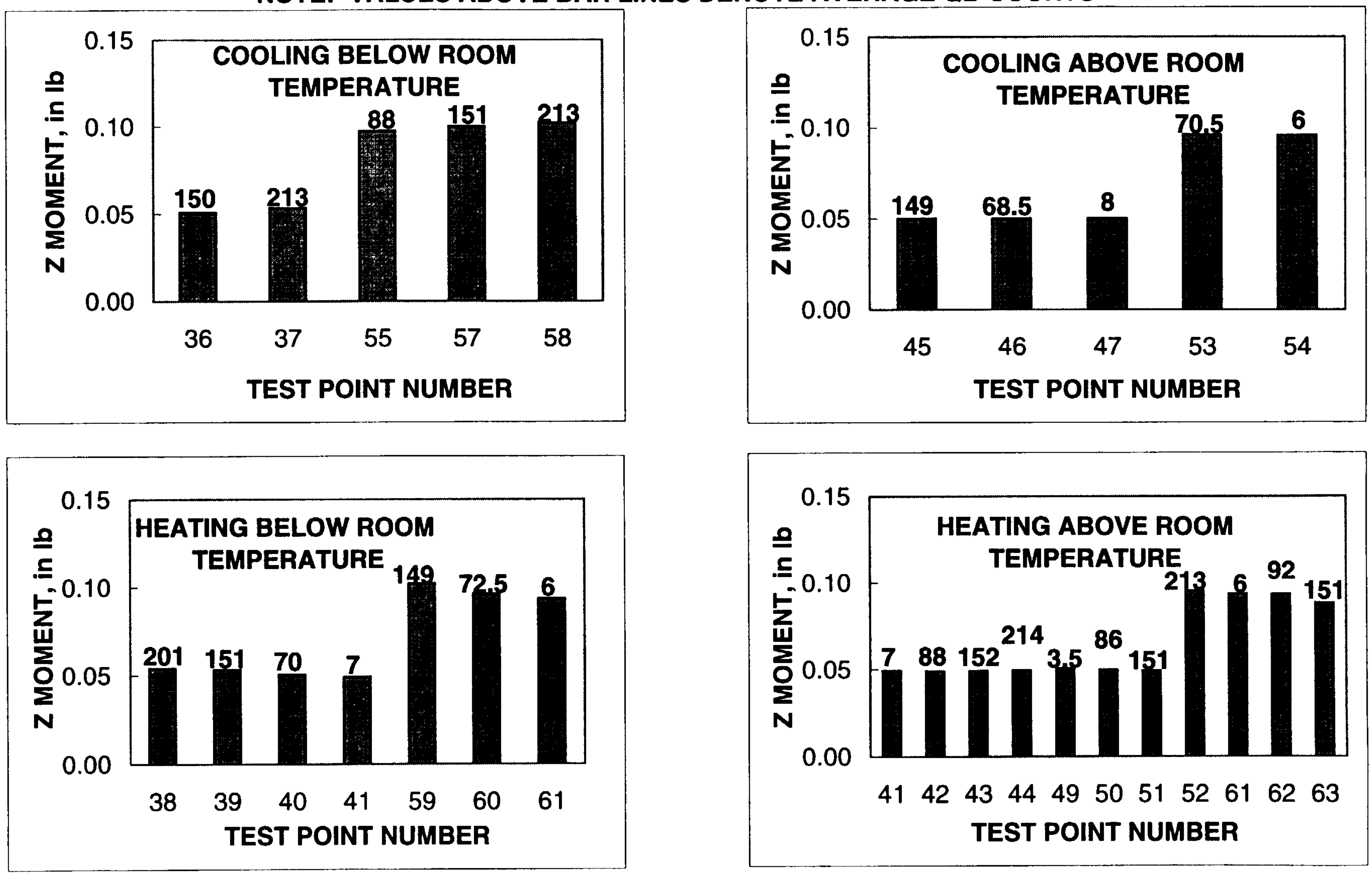

Figure 31. - Z Moment - One Third Octave Center Band Frequency = 63 Hz

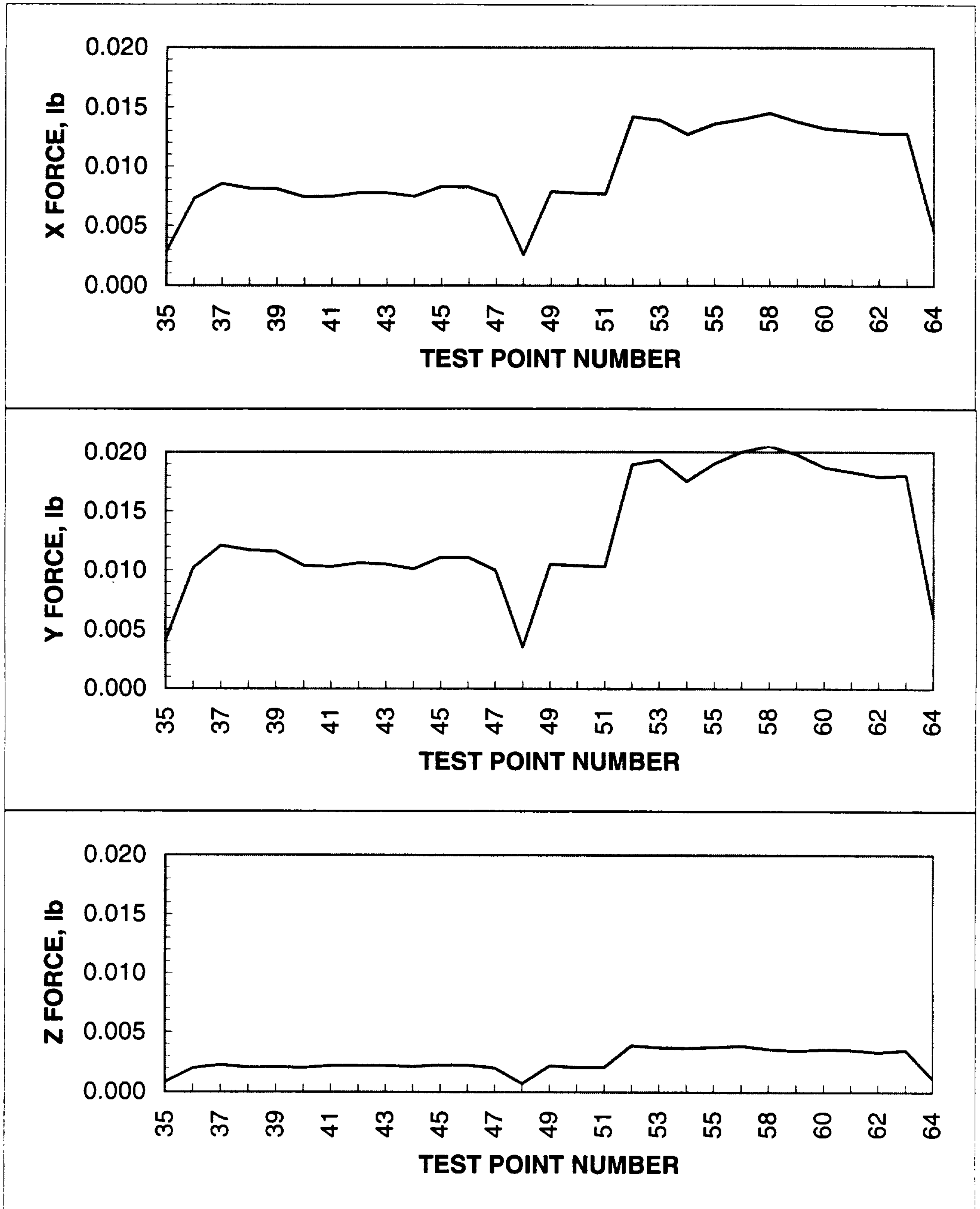

Figure 32. - CRIM Peak Forces at Fan Speed Frequency

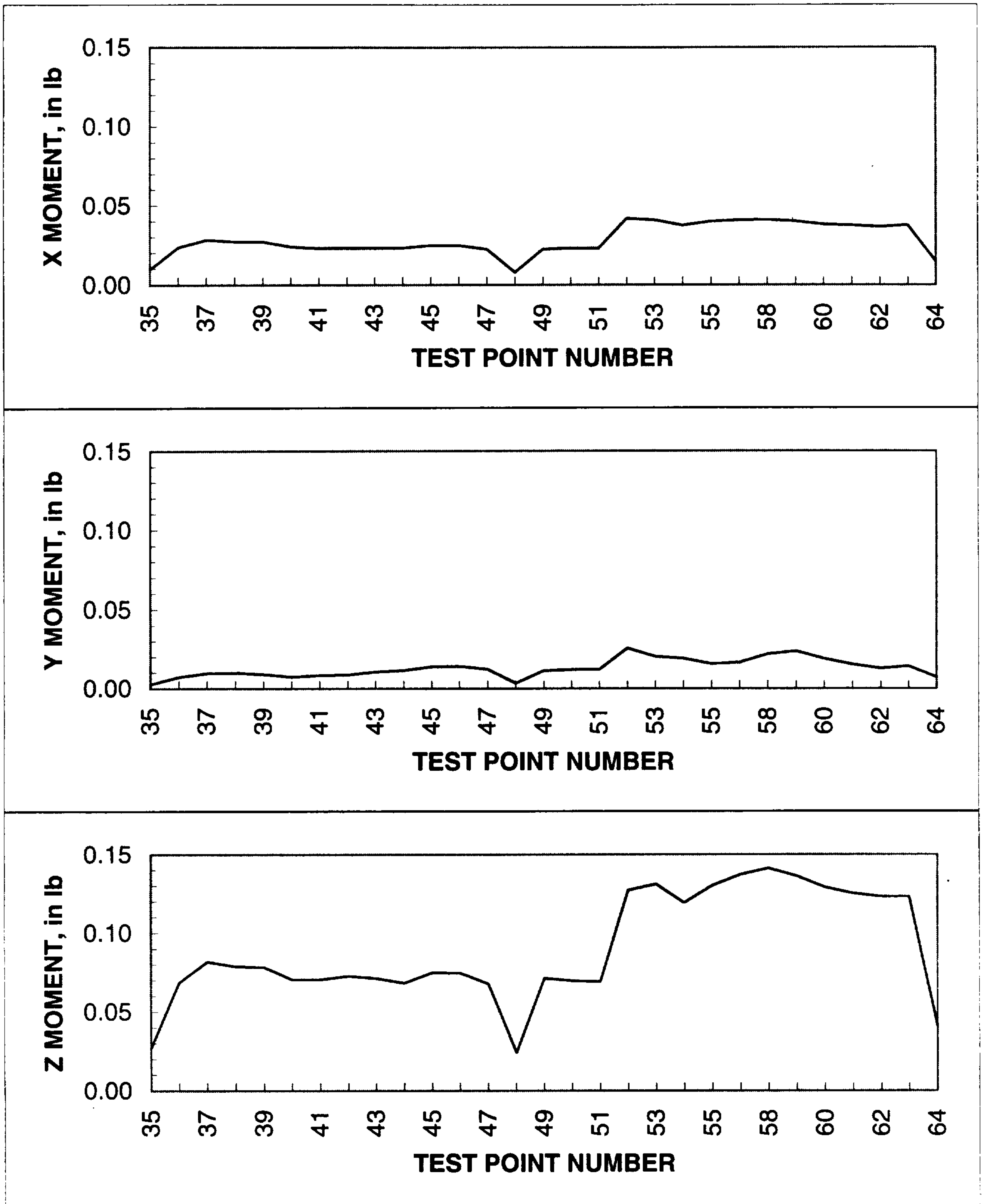

Figure 33. - CRIM Peak Moment at Fan Speed Frequency

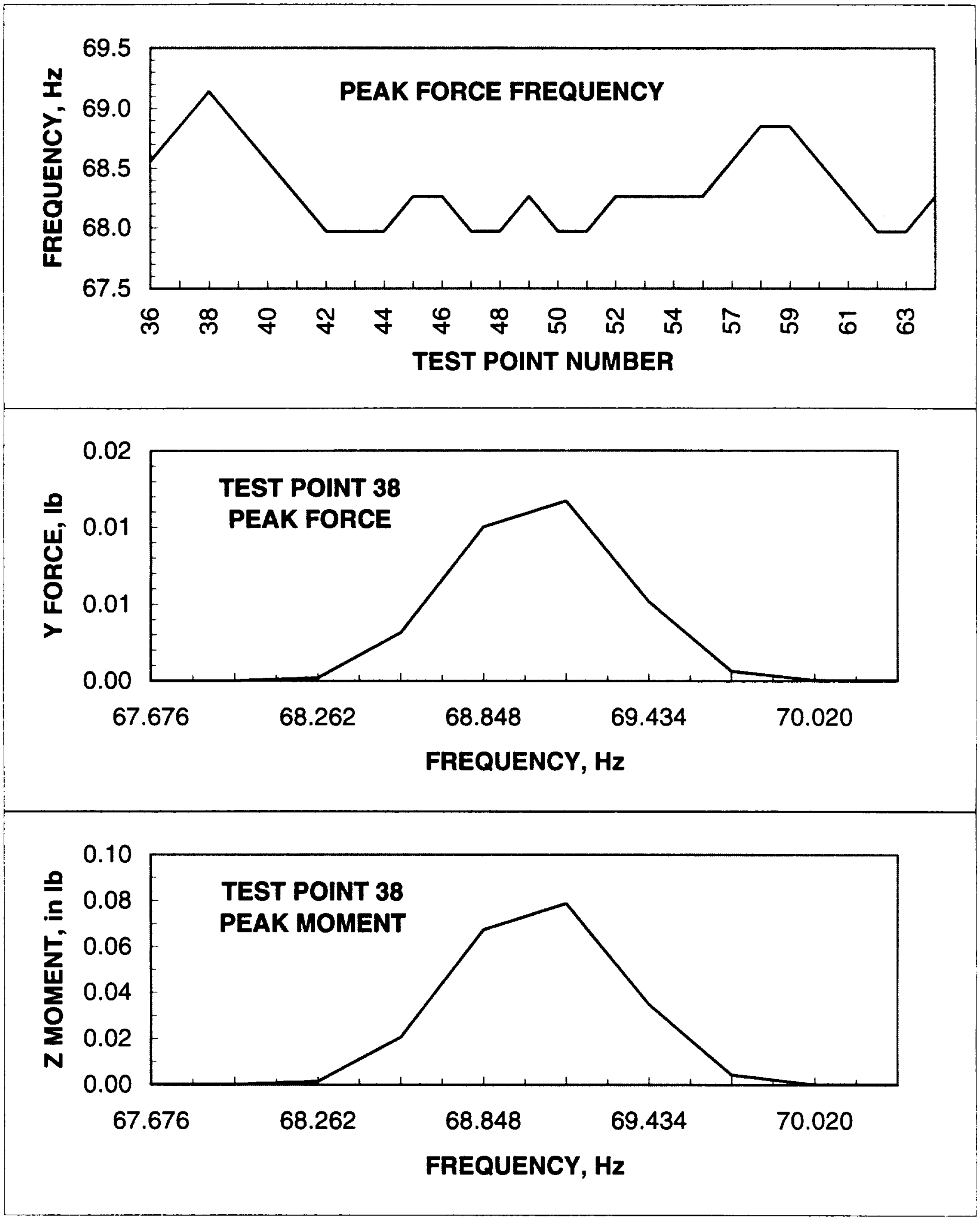

Figure 34. - CRIM Peak Force Characteristics

REPORT DOCUMENTATION PAGE

Form Approved
OMB No. 0704-0188

1. AGENCY USE ONLY (leave blank)

2. REPORT DATE
May 1997

3. REPORT TYPE AND DATES COVERED
Contractor Report

4. TITLE AND SUBTITLE
Low Frequency Vibration Characteristics of the Commercial Refrigeration / Incubation Module

5. FUNDING NUMBERS
C NAS1-19000
WU 963-89-00-01

6. AUTHOR(S)
James W. Russell
Mehzad Javeed

7. PERFORMING ORGANIZATION NAME(S) AND ADDRESS(ES)
Lockheed Martin Engineering and Sciences
c/o NASA Langley Research Center
Mail Stop 371, Hampton, VA 23681-0001

8. PERFORMING ORGANIZATION REPORT NUMBER

9. SPONSORING / MONITORING AGENCY NAME(S) AND ADDRESS(ES)
National Aeronautics and Space Administration
Langley Research Center
Hampton, VA 23681-0001

10. SPONSORING / MONITORING AGENCY REPORT NUMBER
NASA CR-201696

11. SUPPLEMENTARY NOTES
Langley Technical Monitor: Mr. George F. Lawrence

12a. DISTRIBUTION / AVAILABILITY STATEMENT
Unclassified-Unlimited
Subject Category - 18

12b. DISTRIBUTION CODE

13. ABSTRACT (Maximum 200 words)
This report summarizes the results of mass property measurements, and force and moment measurements of the Commercial Refrigeration /Incubation Module (CRIM) over the frequency range from 0.35 Hz to 300 Hz. The vibration test results showed that the primary forces and moments occurred at frequencies between 68 Hz and 69 Hz, which is the operating speed of the fan that controls the airflow. The results also showed that the operating regime of the CRIM and the operating mode of the banks of thermoelectric devices did not significantly affect the maximum forces and moments associated with the fan operating speed. The peak force of 0.021 pounds occurred on the Y axis and the maximum moment of 0.14 inch pounds occurred on the Z axis. The results also show an anomaly in the CRIM force and moment measurements. The forces and moments associated with test points taken after the CRIM was turned off and turned back on due to a thermal fuse overload, were significantly higher than the forces and moments associated with test points taken prior to this shutdown. It was recommended that additional testing be performed on the CRIM to investigate this phenomenon.

14. SUBJECT TERMS
Commercial Refrigeration / Incubation Module force; vibration force; acceleration measurement; microgravity measurement

15. NUMBER OF PAGES
58

16. PRICE CODE
A04

17. SECURITY CLASSIFICATION OF REPORT	18. SECURITY CLASSIFICATION OF THIS PAGE	19. SUCURITY CLASSIFICATION OF ABSTRACT	20. LIMITATION OF ABSTRACT
Unclassified	Unclassified	Unclassified	UL